https://doi.org/10.5194/egusphere-2025-1923
Preprint. Discussion started: 5 June 2025

Integrating Fireline Observations to Characterize Fire Plumes During Pyroconvective Extreme Wildfire Events: Implications for Firefighter Safety and Plume Modeling

Marc Castellnou Ribau[1,3], Mercedes Bachfischer[1], Marta Miralles Bover[1], Borja Ruiz[1], Laia Estivill[1], Jordi Pagès[1], Pau Guarque[1], Brian Verhoeven[2], Zisoula Ntasiou[4], Ove Stokkeland [5], Chiel Van Heerwaarden[3], Tristan Roelofs[3], Martin Janssens[3], Cathelijne R. Stoof [3] and Jordi Vilà-Guerau de Arellano[3]

[1] GRAF. Catalan Fire and Rescue Service. Spain.
[2] Netherlands Institute for Public Safety
[3] Wageningen University & Research
[4] Hellenic Fire and Rescue Service, Greece.
[5] Grenland Fire and Rescue IKS. Norway.

Correspondence to: Marc Castellnou (mcastellnou@gencat.cat)

Abstract. Firefighter entrapments occur when wildfires suddenly transition into extreme wildfire events (EWEs). These transitions are often caused by pyroconvective fire-atmosphere coupling, triggered by a combination of high fire intensity and atmospheric vertical thermodynamic structure. Pyroconvection indices calculated using coarse atmospheric modeling data crudely detect these dynamic transitions due to highly localized atmospheric processes and changes in atmospheric conditions caused by the fire. Consequently, fire managers may remain unaware that fire behavior intensification due to fire-atmosphere coupling is outdating the safety protocols in place. This study presents a new in-plume profiling methodology to improve the assessment of fire-atmosphere interaction dynamics in real-time. As proof of concept, we analyzed 156 in-plume sondes launched during the 2021-2025 fire seasons in Spain, Chile, Greece, and The Netherlands. As a strategy to measure the coupling fire-atmosphere, we propose simultaneously launching two radiosondes: one to measure ambient conditions and another to capture data within the plume updraft. Comparing these profiles, we measure in-situ and in-real time the modification of state variables by the fire-atmosphere interaction. These new observations and methodology improve our assessment of pyroconvection dynamics demonstrating practical implications that support their use by incident management teams. It has the potential to enhance awareness of possible near-accidents and tactical failures during extreme pyroconvective wildfire events. Additionally, it offers a comprehensive observational dataset to improve pyroconvection nowcasting and advance research on fire-atmosphere interaction.

1 Introduction

Pyroconvection is a key driver in the escalation from wildfires to extreme wildfire events. While dry convection plumes effectively accelerate fire spread and produce long-distance spotting, it is the development of *moist* pyroconvection plumes by the formation of pyrocumulus and pyrocumulonimbus (pyroCu/Cb, AMS, 2023) that dramatically intensifies fire behavior. Deep pyroCu/Cb events amplify dry pyroconvective plume dynamics through powerful indrafts and downdrafts, triggering chaotic surges in spread rate, increasing massive and long-range spotting on the head and flanks, and generating deep flames and vortices (McRae et al., 2015; Peterson et al., 2017). These rapid, unpredictable changes surprise and overwhelm responders with no time to react, undermining suppression tactics and leaving little time to react. The onset of moist pyroconvection poses a severe risk to both responders and civilians, as tragically demonstrated by the history of deadly entrapments under such conditions (Cardil and Molina, 2015; Cruz et al., 2012; Lahaye et al., 2018; Page et al., 2019).

The conditions favoring such destructive wildfires are increasing due to climate change and human policies in landscape and fire management (Cunningham et al., 2024; Di Virgilio et al., 2019; Turco et al., 2018; Wilmot et al., 2022). Firefighters must prepare to better detect pyroconvection transitions.

https://doi.org/10.5194/egusphere-2025-1923
Preprint. Discussion started: 5 June 2025

Safety on the fireline hinges on effectively predicting fire spread, particularly by understanding conditions that have previously led to entrapments after sudden fire behavior changes (Wilson, 1977). Insights from these experiences have shaped protocols and orders to enhance crew awareness and prevent future incidents (Ziegler, 2007). The LACES protocol condenses critical lessons into the memorable acronym: Lookout, Awareness, Communications, Escape Route, and Safety Zone (Gleason, 1991). In this framework, the lookout observations and awareness of pyroconvection conditions using indices and models play a vital role. However, transitions in pyroconvection, especially those involving pyroCu/Cb clouds, are affected by highly localized surface and free tropospheric processes, which are hard to predict (Peterson et al., 2017). This complexity makes real-time monitoring of fire plumes and their environment from the fireline a difficult, yet essential safety measure to prevent accidents and fatalities.

Since the 1950s, fire managers have conducted ambient radiosonde profiling to assess the in-situ pyroconvection potential (McCutchan, 1982) during big wildfire events. Using the profiles, the Haines index (Haines, 1989) has become vital for informing firefighters about pyroconvective extreme fire risks, despite its limitations and loss of sensitivity (Potter, 2018).

The analysis of fire-atmosphere coupling has progressed to evaluating temperature as a function of pressure on skew-T diagrams to gauge pyroconvection potential (Goens & Andrews, 1998). This method is based on the observation that wildfires producing pyroCu/Cb clouds often occur in a well-mixed convective boundary layer and moist mid-troposphere, forming the basis for pyroconvection analysis using the parcel method (Jenkins, 2004; Lareau and Clements, 2016; Tory et al., 2018).

The advent of regional and global atmospheric models has transformed this practice, enabling predictions of pyrocloud occurrence through various indices, including convective available potential energy adapted to wildfires (fireCAPE) (Potter and Anaya, 2015), the maximum integrated buoyancy (Leach and Gibson, 2021), and the pyroCu firepower threshold, PFT (Tory and Kepert, 2021).

Nevertheless, the coupling between fire and a turbulent atmosphere is much more complex than can be captured by single indices of the ambient environment. The increase in observations has led to higher-fidelity analyses of turbulent fire plumes (Freitas et al., 2007; Paugam et al., 2016; Rio et al., 2010) and complex fire-atmosphere coupling models such as Meso-NH or WRF-Sfire (Couto et al., 2024; Kochanski et al., 2019). Those models are deepening our understanding of deep pyroconvection and its underlying physics.

A crucial aspect for firefighters is the enhanced understanding that modeling provides regarding the interaction of turbulent plumes with fire spread (Heilman, 2023). This understanding is influenced by factors such as the size of the flaming zone (Badlan et al., 2021), and the dynamics involved in moist pyroconvection (pyroCb) models (Peterson et al., 2017).

However, practical applications for decision-making remain limited, and due to the constantly evolving dynamic relationship between fire and the atmospheric boundary layer, collecting accurate data is essential (Lareau et al., 2024; Prichard et al., 2019). Due to the safety concerns related to operating near extreme fire fronts, data is primarily gathered through experimental-fire campaigns such as FireFlux or RxCadre (Benik et al., 2023; Clements et al., 2015, 2019) involving low to moderate-intensity fires, missing complex and fast-transitioning pyroconvective events. More recent campaigns focus on wildfires to collect more extreme fire behavior (Clements et al., 2018; Rodriguez et al., 2020). Innovative measurement methods such as UAVs (Brewer and Clements, 2020; Koch et al., 2018) and radar (Lareau et al., 2022; McCarthy et al., 2019) are tested to allow better data collection during ongoing extreme fires. Nevertheless, challenges remain during active fires, including issues related to mobility, safety, funding, and data processing.

We aim to develop a fireline data-gathering methodology using in-plume radiosondes with two main objectives: (a) to advance the understanding and representation of pyroconvection and its impact on extreme fire behavior, and (b) to provide fire managers with a real-time tool for assessing the likelihood of occurrence of different pyroconvection prototypes (Castellnou et al., 2022).

https://doi.org/10.5194/egusphere-2025-1923
Preprint. Discussion started: 5 June 2025

Despite observing state variables profiles by means of sondes have been used for decades, their use in wildfire updrafts for real-time comparisons with ambient profiles is challenging. We need to assess if the uncontrolled ascent trajectory of a sonde can capture plume height, state variables, and help evaluate pyroconvection characteristics. It is vital to evaluate their reliability across different fire intensities. By obtaining accurate vertical profiles of ambient and in-plume updraft conditions during the early stages of fire growth, we seek to capture plume-driven modifications in the state variables. This will help raise awareness of pyroconvection conditions and their likelihood of leading to an EWE.

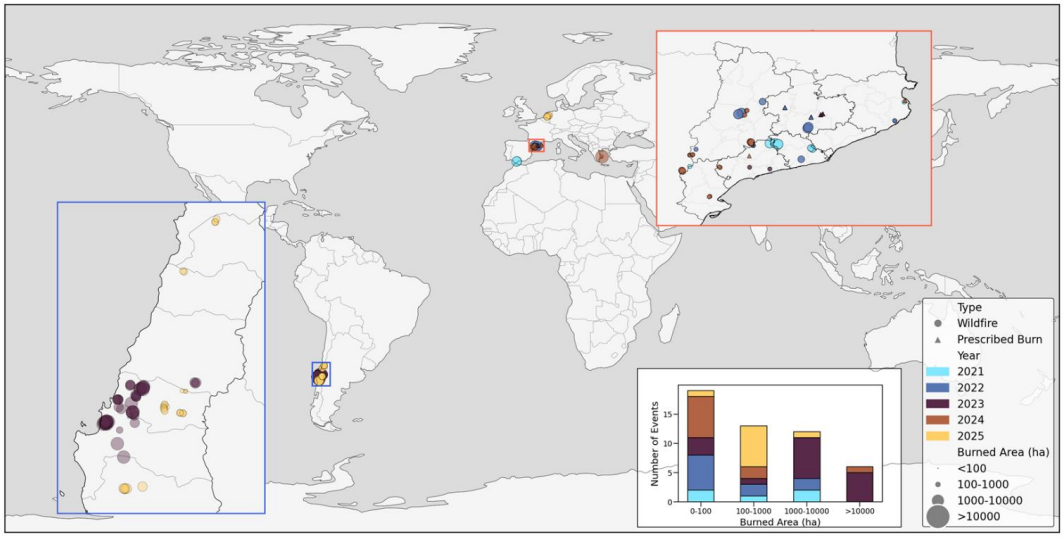

Figure 1: Location of the 156 in-plume profile observations during the radiosonde campaigns conducted between 2021 and 2025. Sondes are identified based on whether they were launched during wildfires (circle) or prescribed fires (triangle). The sondes are distinguished by whether they were launched during wildfires (circles) or prescribed fires (triangles). The color of each dot represents the campaign year, while the size of the dot reflects the total fire size (in hectares). The distribution of fire sizes is shown in the bar plot to highlight the range of fire sizes in which the methodology has been tested. Last updated: April 23, 2025.

2 Methodology

To develop a methodology for assessing pyroconvection during wildfire operations and to create a valuable dataset for improving models and research, we conducted field campaigns from 2021 to 2025 in Spain, Chile, Greece, and the Netherlands, launching 156 in-plume sondes during active fires (Figure 1).

This approach was crafted through collaboration among firefighters, fire scientists, and meteorologists, prioritizing team safety and consistent data collection.

We detail the methodology, focusing on safety protocols, coordination, equipment selection, launching procedures, and data collection for vertical profiles in ambient conditions and plume updrafts.

2.1 Field campaigns

Our efforts focused on helping fire managers detect potential transitions from pyroconvection to pyroCu/Cb. To achieve this, we need to test our methodology and launch sondes during the early stages of wildfire development, when pyroconvection is being initiated, and the plume is still a surface or convective plume.

We aimed at a wide range of fire sizes (bar plot in Figure 1), testing our methodology on both low-intensity prescribed fires (14.7%) and active wildfires (85.53%). Specifically, we targeted wildfires that have the potential to transition to pyroconvection during peak fire seasons: July to September in Mediterranean Europe (ME, 44.73%), March to May in Atlantic

https://doi.org/10.5194/egusphere-2025-1923
Preprint. Discussion started: 5 June 2025

Europe (AE, 3.29%), and January to March in South America (SA, 51.98%). We considered all types of vegetation, including cereal fields/grasslands (16.2%), brushlands (40.5%), and forests (43.2%).

2.2 Safety and coordination

Moving within the fire area requires adherence to safety protocols and coordination with the incident management team. We recommend deploying a sonde crew consisting of at least two members: a lookout and a launcher. This team will gather data and implement a LACES protocol with an emphasis on awareness.

Clear communication between the launching team and aerial resources coordination is crucial to ensure safety with fire suppression helicopters and air tankers. The small colored sondes are safe for aircraft if their launch timing and position are known, as they mainly travel within the updraft of the plume, where aerial resources don't operate.

Before the launch, the team must select the Escape route and the Safety zone based on the expected fire behavior (Butler, 2014). These locations must be shared with the nearby firefighters, as they will be utilized for rescue efforts if necessary.

2.3 Equipment

Capturing information on the ongoing fire-atmosphere coupling to assess safety for firefighters requires equipment that is capable of real-time and in-situ pyroconvection assessment. To select the most suitable method, we compared the characteristics of five meteorological measurement techniques, namely professional high-altitude weather balloons, small weather balloons, doppler radar, unoccupied aerial vehicles (UAV), and helicopter sensors. Our requirements are as follows:

- Light, mobile equipment suitable to operate near the flame front and entirely operated by one person; a second person is only required for safe mobility and fire monitoring (lookout).
- Fast: deployment within 5 minutes.
- In-situ and real-time information acquisition on the fireline, ready for immediate decision-making.
- Safe for operating along with aerial resources.
- Provision of two vertical profiles, one outside the fire's range of influence on the atmosphere, and one inside the fire plume to obtain the fire-modified vertical profile.
- Simultaneous, or ensemble measurements of atmospheric vertical profile thermodynamics up to lifting condensation level (LCL).
- Low cost: Affordable for the budget of firefighter crews.
- Low complexity: Implementing the methodology should be accessible and not require complex technical skills and knowledge

Table 1: Requirements for safe deployment in active wildfires and for providing real-time information on thermodynamic atmospheric profile conditions. Small balloons are the only equipment that meets all the specified requirements.

	Professional high-altitude balloons	Small balloons	Radar Doppler	UAV-drones	Helicopter sensors
Max 2-people needed	X	X		X	
< 5 min deployment	X	X		X	X
Real-time info	X	X			
Safety for aerial resources		X	X		X
In fire/out fire profiles	X	X		X	X
Simultaneous measurement		X	X	X	X
Low cost		X			
Ease of use	X	X			

https://doi.org/10.5194/egusphere-2025-1923
Preprint. Discussion started: 5 June 2025

Comparison of professional high-altitude balloons, small balloons, radar doppler, UAV-drones, and helicopter sensors (Table 2) indicate that most tools were unreliable for rapid deployment in the fireline and provide real-time data with safety . The only exception are small balloons, which meet all the requirements listed above, and are safe enough for aerial resources in the unlikely case that the sonde travels near an aircraft.

We therefore selected a small helium balloon (60 liters), namely the light radiosondes model S1H2 (12 gr) from Windsond (Figure S1) to develop a measurement kit. The system has been previously tested against larger, professional radiosondes and successfully achieved relevant measurements, despite its weaknesses in GPS processing and humidity response time at cloud tops (Bessardon et al., 2019). Previous research that we conducted during active wildfire events demonstrated that these challenges did not hinder the detection of pyroconvective phenomena (Castellnou et al., 2022).

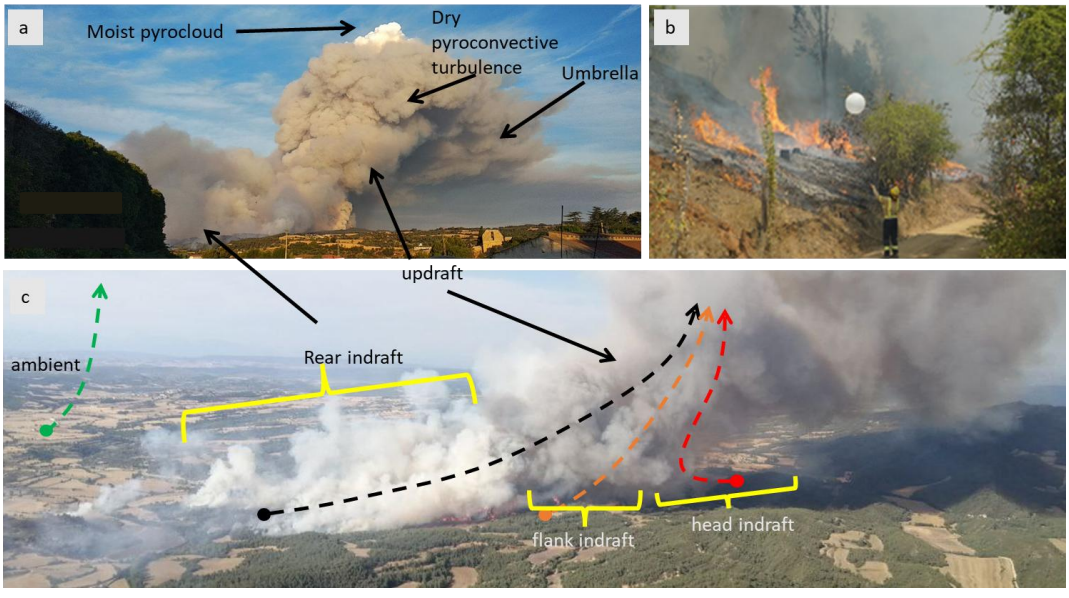

Figure 2: Sonde launching within the fire plume area. a) plume description from an upwind location. b) detail of a sonde launching (see video S2.1 and S2.2). c) Launching locations relative to the indraft induced by the plume updraft. The black dashed arrow represents a rear indraft sonde, the orange dashed arrow represents a flank indraft sonde, the red dashed arrow represents a head indraft sonde, and the green dashed arrow represents the ambient sonde away from the plume's influence. This panel illustrates the key characteristics of a plume: the updraft, which conforms the chimney; the dry pyroconvection turbulence, inside the ABL and forming the grey smoke turbulence at the chimney's peak; the moist pyrocloud, defined by LCL and identified by where condensation occurs, typically forming pyrocumulus or pyrocumulonimbus clouds (pyroCu/Cb); and the umbrella, a dense layer of smoke that forms around the top of the updraft and extends downwind into the injection layer.

2.4 Strategy of the launching procedure

Our strategy and primary objective were to systematically obtain (1) an ambient sonde outside the shading of the plume and (2) an in-plume sonde, launched close enough to the plume into the indraft, capturing the fire-induced changes in the atmospheric boundary layer (ABL). Both soundings should be taken no more than 1 hour apart (Figure 2).

- Framing the day vertical atmospheric profile conditions:

We utilize the ICON-EU 7*7 km^2 resolution simulated atmospheric vertical profile to understand the general conditions we can expect (https://www.dwd.de/EN/ourservices/nwp_forecast_data/nwp_forecast_data.html).

- Criteria for maximum height sonde ascent:

https://doi.org/10.5194/egusphere-2025-1923
Preprint. Discussion started: 5 June 2025

We aim to reach altitudes defining the ABL and LCL before terminating the sonde for recovery. Given the elevated plume-modified LCL height (Lareau & Clements, 2016), the balloon cut-off height is set at a minimum of 1000 m above the theoretical LCL, as indicated by atmospheric model data.

- Balloon filling-up:

We use a helium-pressurized container and a manometer installed on the fire service vehicle, systematically using 60 liters of helium to ensure the balloons have consistent characteristics.

- In-plume or updraft sonde:

Launched near the flame front into the plumes' indraft, the device measures state variables affected by the fire-atmosphere interaction. However, turbulence around the head of the fire can significantly impact the readings. To address this issue, we classified each updraft sonde based on its position relative to the plume's indraft, using categories: head indraft (downwind from head fire front), flank indraft (on the flanks), or rear indraft (upwind from the head fire front) launching positions (Figure 2). This classification ensures interoperability among sondes of the same kind of indraft.

- Ambient sonde:

Launched outside the fire influence (Figure 2), it measures the vertical profile of the state variables in an environment uninfluenced by the fire plume.

Although launching a separate ambient sonde is recommended, our campaign findings indicate that an ambient profile can also be obtained from the in-plume sonde descent path if the sonde is cut-down once it is outside the plume's influence. By comparing data from both the in-plume descent and the ambient sondes, we can improve the reliability of our findings.

2.5 Ambient, plume updraft, and fire spread data

2.5.1 Data collection for real-time monitoring of fire-atmosphere interaction

- In-situ radiosondes data (ambient and in-plume): The vertical profile variables (Table 2) of temperature T^a (K), relative humidity RH (%), horizontal wind U ($m \cdot s^{-1}$), and sonde rising velocity ($m \cdot s^{-1}$) are retrieved at a 1-second resolution. Here, we use the sonde rising velocity as a proxy for vertical wind speed (w). The data is transformed to state or conserved variables: specific humidity q ($gr \cdot kg^{-1}$), potential temperature θ (K), and virtual potential temperature θv (K) (Appendix S3).
- Instantaneous Fire Spread.
    - Observed rate of spread (ROS, $m \cdot s^{-1}$).
    - Size of the head flaming zone and deep flame (m^2).

2.5.2 Data collection for post-analysis and research

- Radar measured echotop. It is a proxy measure for the plume top. We analyze the radar echotop height (m) using radar data from the Servei Català de Meteorologia (www.meteo.cat). We filter the radar echotop data and define the estimated plume top as the maximum height where the reflectivity value equals or is higher than 12 dBZ. Unfortunately, the data for all fires is not available. This dataset is utilized to validate the estimates of plume tops collected from in-plume radiosondes during 18 wildfires.
- Atmospheric model data: The same variables measured by the sondes are obtained from ICON-EU 7*7 km horizontal resolution and for hourly timesteps. The model data is interpolated to obtain a vertical profile with a 10 m resolution.
- Overall Fire Spread.
    - Fuel type (Scott and Burgan, 2005): We record the dominant fuel type to be used in Heat Flux modeling.
    - Fire isochrones. Produced by the Fire Service, it allows us to compute the rate of spread (ROS, $m \cdot s^{-1}$) as the maximum distance in the wind direction between two consecutive hourly isochrones (Duane et al., 2024).

https://doi.org/10.5194/egusphere-2025-1923
Preprint. Discussion started: 5 June 2025

- Heat Flux: Using ROS and knowing the fuel type we estimate the heat flux ($kW \cdot m^{-2}$) and the fireline intensity FLI ($kW \cdot m^{-1}$) (Finney et al., 2021; Rio et al., 2010).
- Fire Radiative Energy (FRE, TJ): Satellite-measured energy emitted by the fire (TJ) allows us to obtain a directly measured heat flux. However, this measure is unreliable for low-intensity and small fires due to limitations in spatial and intensity resolution(Wooster et al., 2021).

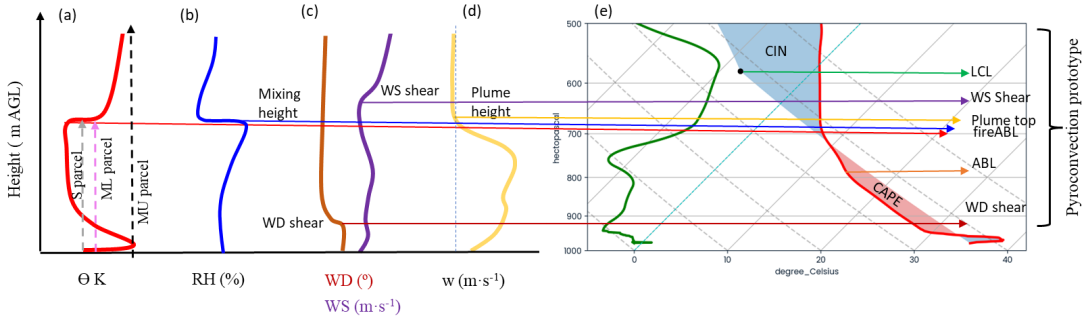

Figure 3: Characterizing wildfire dynamics with respect to ABL dynamics. A theoretical-sounding data representation is used to schematize the criteria to inspect radiosounding variable profiles visually. a) Θ profile is used to obtain the potential parcel heights as a proxy of the plume height. We show ML, MU and S parcels, initialized using the layer-averaged Θ on the bottom 150hPa of the captured vertical profile, the maximum Θ on the same 150 hPa layer, and the surface Θ respectively. b) RH profile is used to assess the mixing layer height in the plume area. c) Wind direction (WD) and speed (WS) shear are represented to the level of the highest gradient, d) w profile or rise velocity profile is used to assess the plume top when the value after the updraft excess returns to the ambient value. The skew-T diagram using Td and Ts is used to assess ABL and LCL height on the ambient data visually. The proximity of the turbulence levels LCL, ABL, fireABL, WS shear, and WD shear are used to assess the pyroconvection prototype (Castellnou et al. 2022).

2.6 Characterizing ABL dynamics

Below are the criteria used to characterize the wildfire's dynamics with respect to the ABL dynamics (Figure 3). We combine numerical estimations based on physical sounded criteria with a visual inspection of plotted profiles.

- ABL: The height of the maximum RH value is used as a criterion to estimate the height of the atmospheric boundary layer (ABL). This criterion is based on the observation that specific humidity is often well-mixed in the convective boundary layer (CBL), which is typical of fire-spreading conditions, while temperature reduces with height within it. The result is an increasing RH with height, with a peak at the inversion, above which it's drier and warmer, and RH drops (Li et al., 2021; van Stratum et al., 2014; Vilà-Guerau de Arellano et al., 2015).

  We differentiate between the ambient ABL and the updraft fireABL. The latter refers to the thermodynamic changes in the ABL induced by the fire plume and restricted to the plume's area. The fireABL height is often identified by the plume injection height or detrainment level (Castellnou et al., 2022; Moisseeva, 2020).

  Numerically (Appendix S3), the ABL and the fireABL height are complemented by computing them using the bulk Richardson number (Rib) based on the ambient and in-plume profiles (Zhang et al., 2014).
- Wind shear: The height of the maximum gradient in the wind speed (s^{-1}) and direction profiles.
- Measured Plume top: The height at which the rising velocity of the in-plume sonde stabilizes back to the ambient sonde values. Due to the difference in density between helium and air, a sonde in the ambient average lower troposphere is expected to rise between 1.5 and 2.5 $m \cdot s^{-1}$.
- Maximum potential plume top: The height to which the air parcel may rise using the parcel method (Holzworth, 1964; Seibert et al., 2000). We use different parcel definitions following earlier pyrocloud studies (Lareau and Clements, 2016; Tory et al., 2018), initialized at launching height above ground level (AGL, m) and assuming their dry adiabatic ascent. These include the most unstable (MU), the mixing layer (ML), and surface (S) parcels. The MU parcel is

https://doi.org/10.5194/egusphere-2025-1923
Preprint. Discussion started: 5 June 2025

initialized using the highest temperature value within the layer-averaged potential temperature for the bottom 150 hPa of the captured vertical profile. The ML parcel is initialized using the mean temperature and mixing ratio within the same 150 hPa layer. The S parcel reflects the surface temperature trajectory required to trigger moist convection. It is initialized with the standard proposal of +3K (Luderer et al., 2009; Potter, 2005).

- LCL: In the Skew-T diagram, the LCL is identified at the pressure level where a parcel rising dry adiabatically from the surface temperature intersects the mixing ratio line associated with the surface dew point temperature. The mixing ratio represents the mass of water vapor per unit mass of dry air ($g \cdot kg^{-1}$). Numerically, the LCL is computed based on surface values using the METPY library (May et al., 2022). A direct numerical estimation (Appendix S3) can also be provided using the surface and dew point temperature (Bolton, 1980; Romps, 2017).
- CAPE / CIN: The integral of the differences between the theoretical undiluted parcel ascend trajectory (parcel method) and the ambient Ts profile. When plotted, CAPE or convective available potential energy is visually estimated as the area where the Ts parcel trajectory > Ts ambient profile, otherwise, the convection is inhibited (CIN). In this study, we consider the air parcel in the fire front begins its ascent at a temperature and humidity higher than surrounding values and the level of free convection is thus the surface. (Jenkins, 2004).

Table 2: Data Types and Sources Used in In-Situ and Real-Time Plume Pyroconvection Prototype Analysis. The ambient and updraft sonde profile observations serve as the data source for visual estimates of levels and parcel trajectories along the state variable's graphical profile. Information about fire behavior is obtained from the fire service. Meteorological radar measurements are sourced from the Catalan Meteorological Service, when available. Additionally, complementary heat flux measurements are gathered from geostationary satellites.

	Variable	Units	Source
Readings	sonde ascending profile	UTM	Profile observation
	Tª (Ts, Td)	K	Profile observation
	RH (Relative humidity)	%	Profile observation
	Pressure	hPa	Profile observation
	U (wind speed)	$m \cdot s^{-1}$	Profile observation
	w component	$m \cdot s^{-1}$	Profile observation
Variables (S3)	u component	$m \cdot s^{-1}$	Computed from profile observation
	v component	$m \cdot s^{-1}$	Computed from profile observation
	q (specific humidity)	$g \cdot kg^{-1}$	Computed from profile observation
	Θ (potential temperature)	K	Computed from profile observation
Fire-atmosphere interaction (S3 for alternative equations)	Measured plume height	m	Visually displayed on the profile: rise-speed sonde profile stability
			Radar echotop filtered at 12dBZ
	Potential plume height	m	Parcel method (see parcels type below)
	LCL (Lifting Condensation Level)	m	Visually displayed on the Skew-T
	ABL (Atmospheric Boundary Layer)	m	Visually displayed on the profile: Maximum RH on the ambient sonde profile
	fireABL (fire induced ABL)	m	Visually displayed on the profile: Maximum RH value on the in-plume sonde profile
	Wind shear	m	Visually displayed on the wind speed profile
	CAPE / CIN	$J \cdot kg^{-1}$	Visually displayed on the Skew-T diagram
Parcels	S (surface parcel)	K	Ts at the surface
	ML (mixing layer parcel)	K	Ts averaged at lower 150 hPa
	MU (most unstable parcel)	K	Maximum Ts at lower 150 hPa
	FRP fire radiative power	TJ	Obtained from geostationary satellites
	FLI	$kW \cdot m^{-1}$	Obtained from measurements by the fire service

https://doi.org/10.5194/egusphere-2025-1923
Preprint. Discussion started: 5 June 2025

Fire	Heat per unit area	$kW \cdot m^{-2}$	Obtained from measurements by the fire service
	Fire spread hourly isochrones	ha	Obtained from measurements by the fire service
	Fuel type	Fuel model	Scott&Burgan general models: GR (grass), SH (shrub), TU (shrub under trees), TL (litter under tree)
	ROS	$m \cdot s^{-1}$	Obtained from measurements by the fire service
	Altitude	m AGL	Sonde launching points
	Coordinates	UTM	Sonde launching points

2.7 Pyroconvection prototype assessment

EWE are typically distinguished between dry convection, normally wind-driven, and the most extreme moist convective, driven by the deep plumes forming pyroclouds (Rothermel, 1991), which include shallow pyroCu, towering pyroCu, and intense pyroCb (Peterson et al., 2017). By examining ABL dynamics and the plume top position relative to ABL, LCL, and wind shear height (Castellnou et al., 2022), we define six different plume prototypes or regimens (Table 3): those driven by dry convection: surface plume, convective plume, overshooting pyroCu, and those driven by moist convection: shallow pyroCu, towering pyroCu, and PyroCb.

As an example, and based on Table 3 criteria, the schematized example of Figure 3 will be classified as a dry convective plume due to the LCL/ABL ratio >>> 1 and the wind shear away from the ABL top.

Table 3: Definition of Pyroconvection dry and moist prototypes. By examining the relative position of a plume concerning the ABL, LCL, and wind shear, we can identify different pyroconvective prototypes (Castellnou et al. 2022). Fire-atmosphere interaction can alter the vertical profile of the plume, potentially triggering a transition to a different pyroconvective prototype. Comparing ambient with in-plume state variables profiles and their different LCL, ABL, and wind shear levels helps to be aware of potential pyroconvection prototype transitions. We provide a brief description of how pyroconvection affects fire spread in relation to previous fire behavior.

	Pyroconvective Prototype	Plume top height	LCL/ABL height ratio	Windshear height	Plume Description	Pyroconvection effect on fire spread
Dry pyroconvection	**Surface plume**	< ABL	>>>1	Away from ABL top	Plumes being diluted inside the ABL	
	Convective plume	=>ABL	>>1	Above ABL top	Plume reaching the ABL top and even overshooting into the free troposphere	Adds fire behavior intensification and short distance spotting
	Overshooting pyroCu	>ABL	>1	on ABL top but below LCL	Plumes reach the free troposphere but are limited by wind shear. They create short-living pyroCu pulses	Adds sustained fire spread acceleration and constant short distance spotting. Perimeter elongation
Moist pyroconvection	**Shallow PyroCu**	>ABL	=<1	on ABL top but on top of LCL	Plume reaching LCL but growing pyroCu is limited by stability or wind shear in the free troposphere	Adds extreme fire spread runs. Sudden Perimeter expanssion pulses. Long distance spotting
	Towering PyroCu	>>ABL	=<1	coinciding with ABL top and LCL	Plume reaching LCL and growing deep NOT reaching T^a < -35ºC (Peterson et al., 2017)	Adds Sustained extreme spread and possible downdraft expanding chaotic fire
	Pyrocumulonimbus	>>>ABL	=<1	coinciding with ABL top and LCL	Plume positively reaching LCL, with deep development and T^a < -35ºC	Stablishes sustained chaotic expanding fire behavior, extreme wind due to downdraft, sustained long distance spotting

3 Results of In-situ plume measurements and assessment of pyroconvection potential

We structure the results section as follows: first, we analyze the differences between the atmospheric model profile and the observed in-situ ambient and plume updraft radiosonde profiles. Second, by comparing updraft and ambient in-situ measured state variable profiles, we examine how effectively sondes with small balloons detect the changes due to fire-atmosphere interactions and accurately identify plume tops. Finally, we assess the sensitivity of such analysis in evaluating pyroconvection

https://doi.org/10.5194/egusphere-2025-1923
Preprint. Discussion started: 5 June 2025

conditions. Here, we focus on assessing the sensitivity in dry and moist convection conditions, considering the different updraft launching positions and scenarios with multiple sondes. Special emphasis is placed on assessing the pyroconvection regime prototypes, as described in Table 3

3.1 Atmospheric models profile compared with small ballons ambient and in-plume radiosonde profiling

Figure 4 compares the ICON-EU model profiles with in-situ ambient and in-plume profiles of thermodynamic variables from two early-stage wildfires: Granja d'Escarp (118 ha) and La Selva de Camp (3.2 ha). We use a Skew-T diagram and the S parcel method to evaluate plume ascent relative to the Lifting Condensation Level (LCL) and visualize CAPE (red shadow) and CIN (blue shadow). We aim to validate in-situ measurements using small balloons to effectively provide detailed and complete profile measurements for assessing pyroconvection conditions.

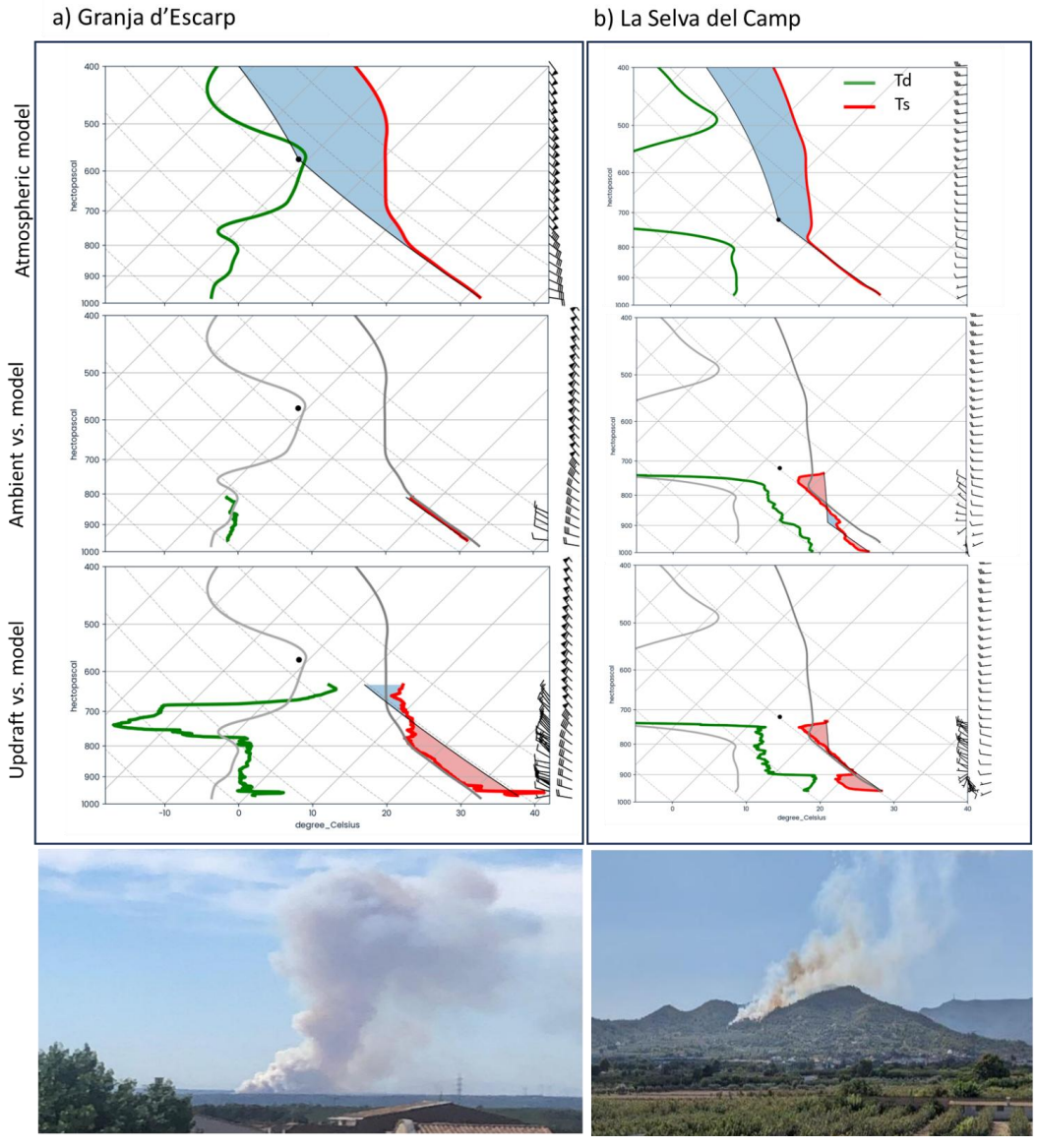

https://doi.org/10.5194/egusphere-2025-1923
Preprint. Discussion started: 5 June 2025

Fire event	Reg	Fuel	in-plume hour (UTC)	Ambient hour (UTC)	area (ha), (Total / hour)	FLI (kW·m^{-1})	ROS (m·s^{-1})	FRE (TJ)	Prototype
Granja d'Escarp 03-07-2024	ME	5	16:37	16:48 16:58	118 / 36	26741	1.05	2.1	Convective
La Selva 2023 03-08-2023	ME	7	15:33	15:50	3.2 / 0.09	1258	0.029	n. d.	Surface

Figure 4: Comparison of atmospheric model, and in-situ ambient and updraft sonde vertical profiles for high-intensity and low-intensity fires. Additional fire information is available in Table S1. **Panel a (left)** presents data for the La Granja Escarp fire (118 hectares) on July 3, 2024. The ICON-EU atmospheric model profile is shown at 17:00 UTC (top), followed by the ambient sonde launched at 16:48 UTC (middle), and the updraft sonde at 16:37 UTC (bottom). **Panel b (right)** provides data for the low-intensity La Selva del Camp fire (3.2 hectares) on August 3, 2023. The ICON model profile is presented at 15:00 UTC (top), the ambient sonde launched at 15:50 UTC (middle), and the updraft sonde at 15:33 UTC (bottom). In the Skew-T diagram, we indicate the S parcel method which also illustrates the Convective Available Potential Energy (CAPE, shown in red shading) and its inhibition (CIN, depicted in light blue shading). Bottom table: wildfire information: Region, total and current hour burnt area (ha), launching hour for in-plume and ambient sonde, Fireline intensity (FLI, kW·m^{-1}), rate of spread (ROS, m·s^{-1}), heat flux captured by satellite infrared sensors (FRE, TJ), and the observed pyroconvection prototype as in Table 3.

Focusing first on the high-intensity La Granja d'Escarp fire (Figure 4a), the intercomparison of the in-plume and ambient observations, and modeling reveal interesting features. The model profile categorized the fire as a convective plume prototype, with a CBL reaching up to 810 hPa and an LCL at 580 hPa. The ambient sounding observed similar characteristics for the CBL and LCL, but it was unable to capture data above the CBL due to the sonde drifting away with the sustained winds. Regarding the in-plume profile, the head-indraft sonde observed marked differences with respect to the two other profiles. At the surface, it recorded an excess of 9 °C and a slightly moister profile. However, a significant drier layer was identified between 790 and 690 hPa. Transported by the plume, the updraft sonde was able to ascend higher than the ambient sonde. On such a profile, the parcel method suggests a potential height of up to 720 hPa and indicates a significant fire-CAPE (red shadow). Despite the potential parcel ascents, the measured updraft temperature difference with the ambient air decreased to below 1 °C at 980 hPa and completely diluted at 790 hPa. The updraft readings suggest no expected change in the convective plume prototype among the three profiles, as reaching the LCL remains unachievable despite the enhanced convective plume.

The La Selva del Camp fire (Figure 4b) was a small fire spreading downhill with low-intensity and showing a fast-diluting surface plume. However, the presence of ambient shallow cumulus clouds associated with sea breeze advection caused firefighters to be concerned about the potential transition into a pyroCu prototype. The absence of local sea breeze advection in the atmospheric model profile accounts for the significant discrepancies observed between the atmospheric model and in-situ profile measurements. The atmospheric model profile indicates a deep convective plume prototype up to 790 hPa when we found further ascent inhibited, making the LCL at 720 hPa difficult to reach. In contrast, the ambient sonde detects the local sea breeze, characterized by a specific humidity of 7 g·kg^{-1}, with the LCL now at 880 hPa. This suggests that a shallow pyroCu prototype that could be triggered by an S parcel increase by3°C. Such a temperature increase would overcome the minor convective inhibition (CIN) at 910 hPa and extend a pyroCu up to 730 hPa. The in-plume profile shows a 4°C temperature increase but results in a weak, rapidly diluted surface updraft at 950 hPa. This leads to a plume constrained below the 900 hPa inversion and with the LCL at 820 hPa. The fire's updraft was too weak to reach the LCL, despite an absence of CIN in the theoretical parcel trajectory. Our measurements confirm that transitioning from the weak plume to a shallow pyroCu prototype is possible but unlikely, requiring significant changes in fire behavior to strengthen updrafts, which is challenging under current conditions.

The two examples in Figure 4 represent the additional value of in-situ profile observations, which can be used to adjust the maximum pyroconvection conditions possible by using the parcel method on in-situ plume updraft profiles.

In both high and low-intensity cases, the fire-induced updraft temperature drops quickly below 950 hPa, deviating from the expected maximum parcel ascent. This creates uncertainty about the plume top's location, hindering our understanding of

https://doi.org/10.5194/egusphere-2025-1923
Preprint. Discussion started: 5 June 2025

pyroconvective conditions in relation to the ABL and LCL (table 3). Locating the true diluted plume top is essential for a more accurate assessment.

3.2 Using updraft radiosondes for measuring plume top heigh and plume state variables

To assess the height of the plume top, it is crucial to determine whether the sonde is being lifted within the updraft.
We focus on how much the fire modifies the measured profiles of virtual temperature (Θv) and the rising velocity of sondes. Both are key variables used in detailed wildfire plume models to frame the plume updraft (Freitas et al., 2007; Rio et al., 2010).

In Figure 5, we display the profile of differences in virtual potential temperature (Θv) between paired measurements of updrafts and the ambient sondes. We analyze the sensitivity of these Θv differences profiles to determine the plume top. First, we combine all the in-plume soundings (Figure 5a) and then separate the Θv differences profiles by each indraft launch position (Figure 2). To allow a more systematic comparison, the height for each sonde has been normalized using the height at the sonde profile equals ambient values of both Θv and rising velocity, assuming this represents the plume well-mixed fireABL. When accounting for the differences between all the paired updrafts-ambient sondes trajectories (Figure 5a), we found the expected Θv excess one can expect in a plume updraft. Such an effect is more pronounced in the flank and especially head indraft profiles (Figure 5c and 5d). However, this increment is rapidly diluted after 50% of the profile height.
Interestingly, in the second half of the profile height, we observe some negative Θv differences. This may be explained by the trajectory of a single sonde passing through the turbulent nature of an updraft, which entrains air from the surrounding atmosphere and by evaporation processes related to moisture from burning vegetation. The rear indraft (Figure 4b) shows more instances of no differences or negative differences compared to ambient and flank and head indraft values during its first 40% of the profile height. This rear indraft location corresponds to the main indraft flow into a fire head (Finney et al., 2015).
Overall, while the updraft-ambient Θv profile differences indicate the expected increase of temperature in an updraft, its rapid dilution, even to cooler than ambient values in the upper part of the profile indicates that Θv is not conserved in an updraft, due to entrainment of colder air governing process of the plumes near the surface. The Θv is not consistent as a variable to be used in assessing the updraft height dilution and identifying the plume top.

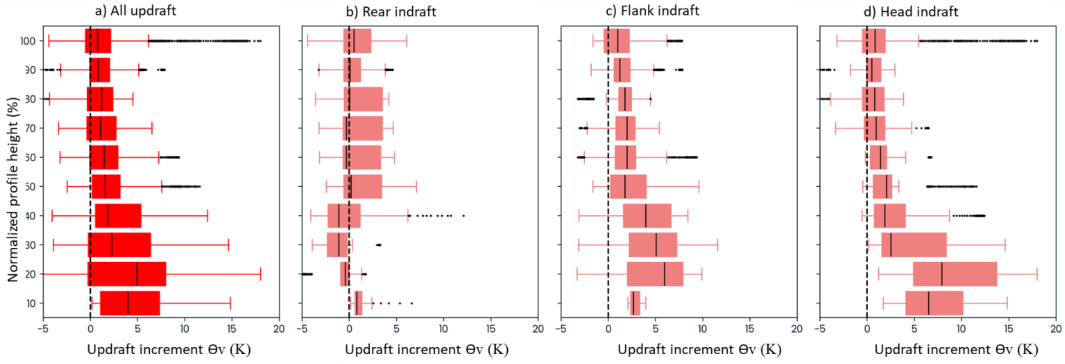

Figure 5: Patterns of differences between updraft and ambient profiles for virtual potential temperature Θv (K). To facilitate intercomparison, each sonde height profile has been normalized with the height when the updraft sonde returns to ambient sonde value or the maximum profile height without descending motion (Castellnou et al. 2022). The zero difference is marked with a vertical black dashed line. We consider four profile types: generic updraft (all updraft profiles), the rear indraft, the flank indraft, and the head indraft (See Figure 2). The temperature profiles are expressed as the difference between the updraft and the ambient profile. None of the updraft profiles differ from each other ($p > 0.005$)

Figure 6 compares the rising velocities profiles for the updraft sondes launched from various indraft positions with those of the collocated ambient sondes. The profile height is normalized, as in Figure 5.

https://doi.org/10.5194/egusphere-2025-1923
Preprint. Discussion started: 5 June 2025

The ambient sonde (Figure 6a) consistently indicates the expected average ascent speed of 2 m·s^{-1} (red dashed vertical line). The most well-defined profile corresponds to the rear indraft (Figure 6b), which in Figure 4 was the profile with less Θv difference between updraft and ambient values. This profile features a consistently accelerated rising velocity beyond 30% of the plume's height. It is the most reliable observation for assessing a vertical profile. In contrast, the sonde on the flank indraft (Figure 6c) is the weakest. Such sondes often take less reliable paths and may only enter the plume at higher altitudes. Some can become entrained in rotating coherent structures, like horizontal rolling vortices (HRV) (Finney et al., 2021), which can occur within intense convective plumes (Figure S4). Conversely, the head indraft profile accelerates rapidly in the lower section, up to 60% of the height, but then loses strength.

Notably, the flank, head, and rear indrafts (Figure 6b, c & d) show the increment in rising velocity that differentiates them from the ambient profile (p=0.005). It is important in the definition of our criteria that the indraft profiles become equal to ambient average rising velocities at 90% of their height. This confirms that the rising velocity vertical profile is a valid criterion to differentiate between in-plume and ambient sondes and identify the plume top when both ambient and in-plume velocities are equal and stabilize around 2 m·s^{-1}.

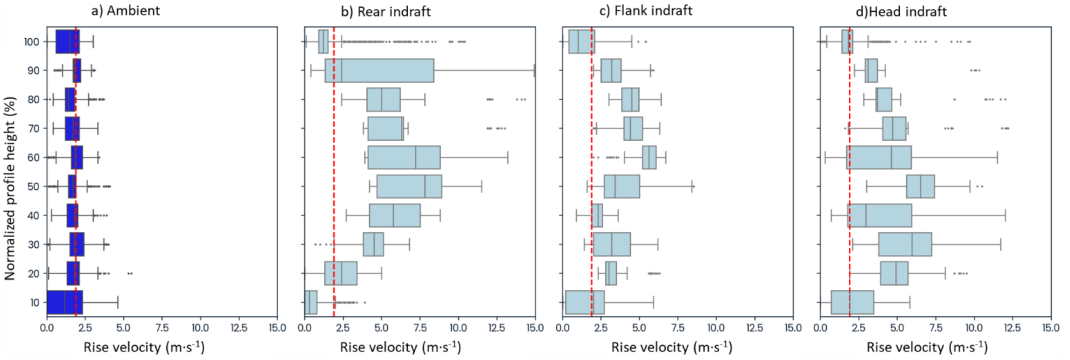

Figure 6: Patterns of rising velocity (m·s^{-1}) vertical profile observed in the updraft sondes. To facilitate intercomparison, each sonde height profile has been normalized with the maximum profile height without descending motion. We consider four profile types: The ambient, the rear indraft, the flank indraft, and the head indraft (See Figure 2). The average ambient sonde rising velocity (2 m·s-1) is marked as a dashed red line. All the updraft profiles are different among them and with the ambient profile ($p < 0.005$). In addition, the profile at 90% of its height returns to the ambient average rising velocity, proposing the vertical speed as an effective variable to read the plume top.

It is important to emphasize that within the first 10% of the height profile for the indraft sondes (Figure 6), the rising velocity is very similar to the ambient values. We analyze these initial ascent moments in Figure 7, comparing ambient and indraft sondes, as they are vital for validating the success of the launch early on. A detailed analysis in Figure 7a reveals that updraft sondes ascend with equal velocities than ambient sondes in a layer between the surface and up to 200 to 300 meters. This pattern has also been observed in profiles from ambient, dry, and moist pyroconvective plumes (Figure 7b), indicating a consistent pattern. The finding resembles a layer at the base of the plume neck represented in plume models as a layer where heat from the fire is dissipated, in contrast to the above layers, where heat transport is actively organized by thermals (Rio et al., 2010).

Based on observational evidence, this layer serves as a guideline for distinguishing updraft radiosondes; beyond this point, the profile can be reliably regarded as different from that of an ambient sonde.

https://doi.org/10.5194/egusphere-2025-1923
Preprint. Discussion started: 5 June 2025

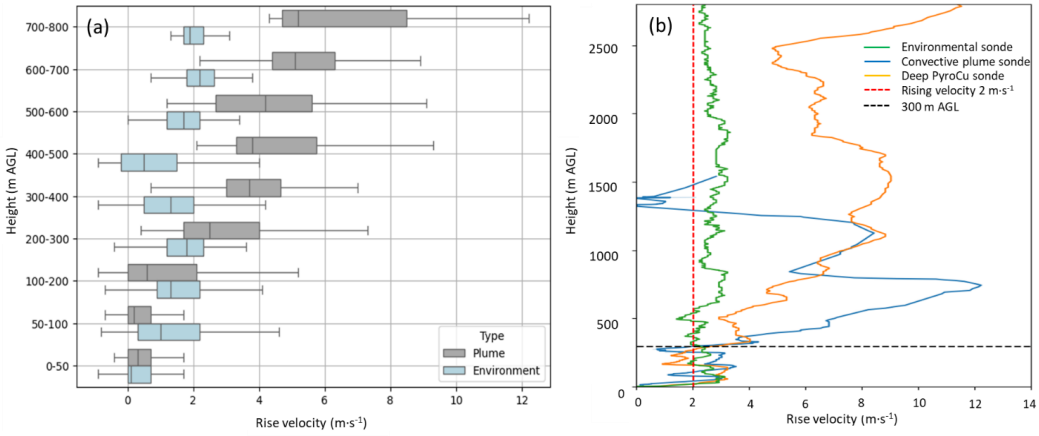

Figure 7: Observations of rising velocities to early differentiation between ambient and in-plume profiles**.** . (a) Boxplot comparing the distribution of rising velocity by height classes (100 m intervals) for ambient (blue) and in-plume (grey) sondes. Ambient sondes maintain a rising velocity of 1.5 to 2 m·s⁻¹ on average, while in-plume sondes accelerate, showing a clear distinction from ambient sondes between 200 and 300 m AGL, with rising velocity exceeding on average the 4 m·s⁻¹. (b) Detailed comparison of single sondes profile for ambient conditions (green), in-plume convective prototype (blue), and pyroCu prototype (orange). The three different cases show the distinctive profile rise velocity acceleration above the identified 300 m threshold.

Based on rising velocities, the previous analysis provided a first-order estimate of the plume's top height. However, independent data is needed to confirm the validity of this estimate. In this context, independent radar measurements are extremely useful for assessing whether the vertical velocity criteria defined in Figure 6 for estimating the dilution plume height , is adequate. Figure 8 shows the correlation between the height at which the rising velocity of the updraft radiosonde returned to ambient values (radiosonde measured plume top) and meteorology radar echotops > 12dBZ (radar estimated plume top). Our dataset included 18 different fires, during which we launched in-plume radiosondes near meteorological radars in Catalonia. The results showed a strong correlation in all cases, with minimal plume top height variations. To complete the analysis, we provide detailed information on two specific radiosondes—one representing moist convection pyroCu and the other representing dry convection plume types (Figure 7b). It was observed that the ascent speed of the sondes decreased significantly as they approached the radar-determined plume top.

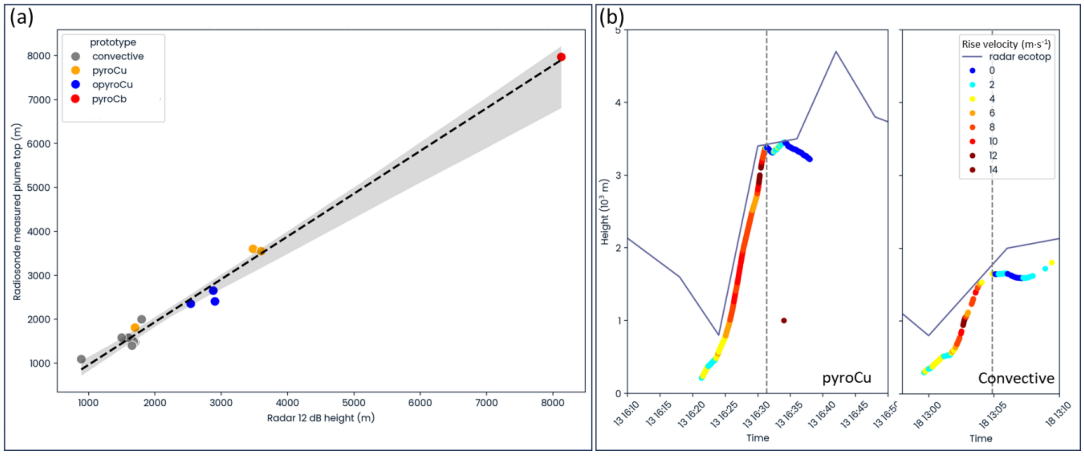

Figure 8: Comparison of plume top height estimate using radar and soundings for different plume type categories. a) Correlation of 18 sondes estimating plume top heights at the same hour and minute as the radar echotop readings at 12 dBZ. The correlation indicates that the vertical profile of rising velocity from the sonde traveling within the plume updraft is a reliable proxy for estimating the plume's top height. b) We compare the radar echotop every 6 minutes with two different updraft sondes rising velocity profiles. The in-plume sonde updraft

https://doi.org/10.5194/egusphere-2025-1923
Preprint. Discussion started: 5 June 2025

profile is colored to facilitate the reading of the rising velocity in $m \cdot s^{-1}$. In both cases, the pyroCu and the convective plume prototype, we observe a close alignment between the sonde estimates and radar readings of the plume top.

3.3 Assessing pyroconvection transitions during ongoing operations

To assess the potential pyroconvection prototype, we compared ABL dynamics differences between collocated in-plume and ambient observed profiles (Table 3). We compare changes in parcel ascent using θv profile. Additionally, we examine how the plume is locally different from the ambient mixed layer height using relative humidity (RH). We analyze wind direction and wind speed shear profiles to understand whether wind is limiting the plume buoyancy. Finally, we determine the current plume top by evaluating the updraft rise speed profile.

We evaluated the sensitivity of the methodology using single sondes in dry convective plumes, moist convective plumes with pyroCu/Cb, and multiple sondes within the same fire.

3.3.1 Dry pyroconvection prototypes

We compare low- and high-intensity fires with dry-convective plume prototypes (Figure 9). The Rojals fire in Spain (Figure 9a) is classified as a surface plume prototype within the ABL (Table 3). The updraft profile, by a head indraft sonde, shows a surface temperature excess of 7 K. However, this increase rapidly dissipates at 300 m before reaching the 420 m AGL of the plume top identified by the rising velocity profile (dashed orange line). The plume does not deepen upon reaching the ABL top, as confirmed by mixing layer height by the relative humidity profile (blue dashed line), which remains unchanged between the ambient air and the plume. This finding is supported by the varying wind shear values observed between in-plume and ambient conditions. Higher wind speeds are noted within the plume compared to the ambient. In this scenario, the theoretical undiluted updraft height, estimated using the MU parcel method (black dashed arrow), is located at 980 m AGL. This value is significantly higher than the current diluted plume top but still 1200 m below LCL. The ML parcel potential height (pink dashed line) coincides with the diluted plume and mixing layer in the inversion at 420 m AGL. We conclude that there will be no transition to a different pyroconvective prototype with these diluted updraft conditions, even if an undiluted updraft can be preserved, as the MU parcel indicates.

The Santa Ana fire in Chile (Figure 9b) is categorized as convective plume prototype. The updraft profile, by a head indraft sonde, shows a temperature excess of 16 K at 130 m AGL. This temperature decreases to ambient values at 780 m AGL. The updraft rising velocity criteria estimates the plume top at 1340 m AGL. Such a measure is confirmed by both the RH profile (thick blue dashed line) proposing a fireABL deepening of 510 m above the ambient ABL (thin blue dashed line) and wind direction changes from the ambient ABL height to the suggested plume top. Notably, the rising velocity steadily decreases as the plume deepens in the stable region above the ambient ABL, where the plume θv becomes up to 4K colder than the ambient sonde. Unlike the Rojals fire, this case shows evidence of a potential transition from a convective plume prototype to an overshooting pyroCu prototype, as suggested by MU parcel. Observing the plume top dilution just below the Lifting Condensation Level (LCL) in real-time is a unique and valuable aspect of this methodology. Thanks to these in-situ profiles, crews left for safety zones, and 2 hours later, the formation of an opyroCu worsened the spread of the fire.

https://doi.org/10.5194/egusphere-2025-1923
Preprint. Discussion started: 5 June 2025

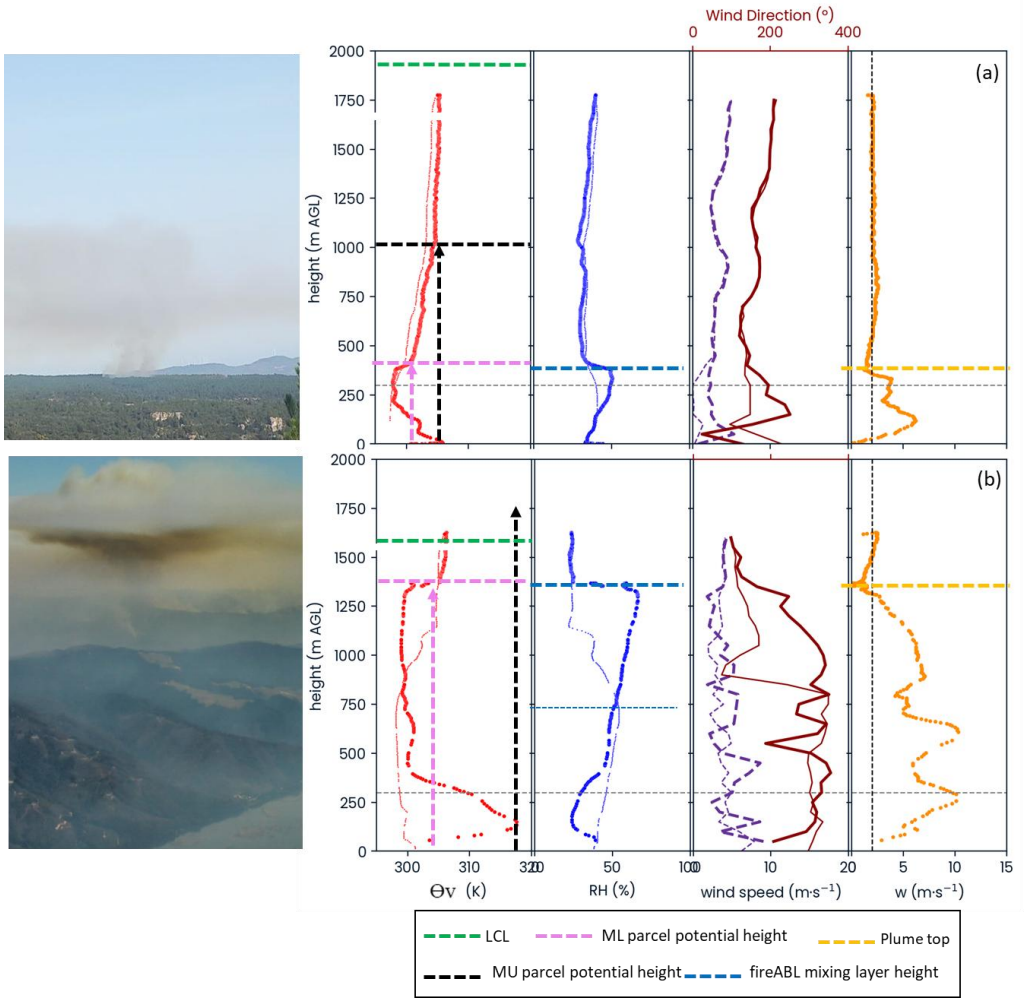

Fire event	Reg	Fuel	in-plume hour (UTC)	Ambient hour (UTC)	area (ha), (Total / hour)	FLI (kW·m^{-1})	ROS (m·s^{-1})	FRE (TJ)	Prototype
Rojals 21-03-2024	ME	TL	14:29	14:49	6 / 0.7	870	0.025	n. d.	surface
Santa Ana 19-02-2023	SA	TU	17:3216:32	16:4617:43	10412 / 736	28974	0.55	14	Convective/opyroCu

Figure 9: Interrelating state variable profiling for dry pyroconvection prototype. a) Rojals fire 2024, Spain. The updraft sonde is a head indraft type. The ambient sonde is launched 2.1 km to the W. b) Santa Ana fire 2023, Chile. The updraft sonde is a head indraft type. The ambient sonde is launched 4.5 km to the E. Profiles use a thin line for the ambient sonde and a thick line for the updraft representing Θv (K, red), Relative humidity (% blue), wind direction (°, violet), wind speed (m·s^{-1}, dark red) and vertical speed w (m·s-1, orange). The Θv profiles include LCL (dashed green). The parcel method potential plume height by ML parcel (dashed pink vertical arrow) and MU parcel (dark dashed vertical arrow) is shown on the Θv. The RH (%) maximum value identifies the mixing layer height. The wind direction and speed profiles identify the wind shear. The rising velocity quantifies plume top heights (dashed orange line) Using the 2m·s^{-1} criteria. The horizontal thin and dashed grey line indicates the 300 m AGL needed to confirm an in-plume sonde, as in Figure 7. Bottom table: wildfire information: Region, total and current hour burnt area (ha), launching hour for in-plume and ambient sonde, Fireline intensity (FLI, kW·m^{-1}), rate of spread (ROS, m·s^{-1}), heat flux captured by satellite infrared sensors (FRE, TJ), and the observed pyroconvection prototype as in Table 3.

3.3.2 Moist pyroconvection prototypes

https://doi.org/10.5194/egusphere-2025-1923
Preprint. Discussion started: 5 June 2025

In Figure 10, we examine the Martorell fire dynamics from 16:00 to 17:30 UTC, during which eight firefighters were trapped due to rapid and unpredictable surface fire spread changes that are closely correlated to the transition from a convective plume into a shallow pyroCu prototype.

At 16:29 UTC (Figure 10a), the in-plume vertical speed profile for the rear indraft sonde indicates a plume rise to 3430 m AGL, a height, 800 m above LCL, and producing a shallow pyroCu prototype. The rising velocity profile boosts at 2620 m AGL from 6 to 12 $m \cdot s^{-1}$, an effect possibly attributable to the latent heat release from the pyroCu condensation (Rodriguez et al., 2020). The RH profile maintains high values (>90%) across the 1000 m deep moist pyrocloud overshoot. Notably, the wind direction profile, initially with shear between 600 and 800 m AGL is changed by the plume to the mixing layer top at the base of the pyrocloud. The resulting plume top by the pyroCu shows a plume height of 120% of the ML parcel expected height (pink dashed line), but similar to the MU parcel maximum potential height. Despite the fire's intensity and observed fireABL modifications, the Θv profile shows minimal difference from the ambient profile, consistent with no Θv excess on the rear indraft profiles (Figure 4). Based on the parcel analysis and the measured profiles indicating an increment in stability and WS shear at the current plume top height, the maximum pyroconvection prototype is likely achieved, and further deepening to pyroCb is difficult to occur.

Half an hour later, the same fire is a downhill and less intense fire below 3000 $kW \cdot m^{-1}$, forming a surface plume prototype. A sonde launched at the head indraft (Figure 10b), identifies the plume top at 1650 m AGL (orange dashed line), a quick diluting updraft from a descending front. The updraft is too weak to reach the LCL. However, the measured updraft Θv profile with an excess of 8 K on the surface proposes a MU and ML ascend above LCL, pointing to a potential transition to a pyroCu prototype It is important to be vigilant about this situation, as changes in fire spread could easily trigger the formation of a shallow pyroCu prototype, which could suddenly intensify the rate of fire spread

https://doi.org/10.5194/egusphere-2025-1923
Preprint. Discussion started: 5 June 2025

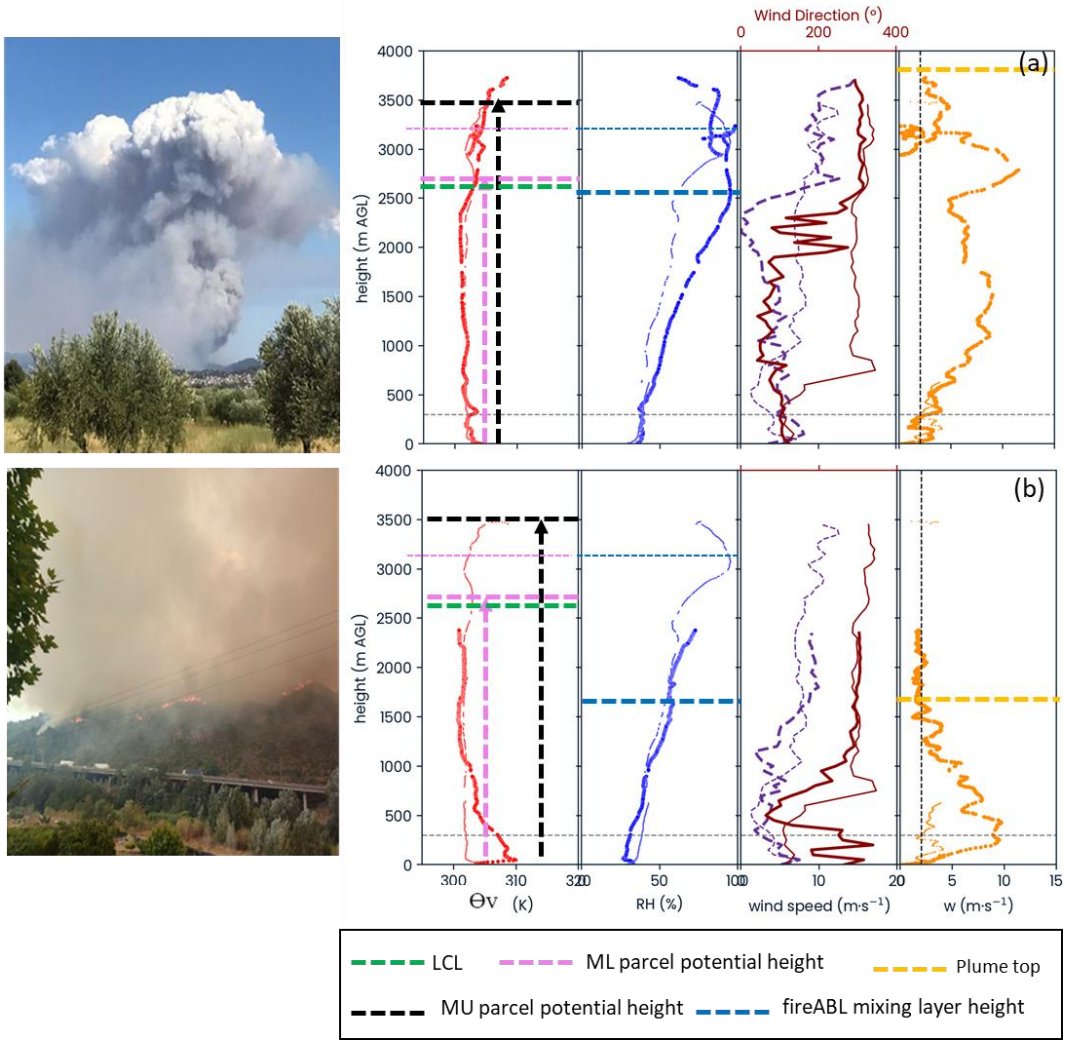

Fire event	Reg	Fuel	in-plume hour (UTC)	Ambient hour (UTC)	area (ha), (Total / hour)	FLI (kW·m⁻¹)	ROS (m·s⁻¹)	FRE (TJ)	Prototype
Martorell 13-07-2021	ME	TU	16:29	16:42	298 / 123	12750	0.61	8.2	pyroCu
Martorell 13-07- 2021	ME	TU	17:02	16:42	298 / 2.6	3000	0.083	1.1	surface

Figure 10: Interrelating state variable profiling for moist pyroconvection prototypes**.** a) Martorell fire 16:29 UTC, Spain 2024 by a rear indraft sonde. b) Martorell fire 17:02 UTC, Spain 2024 by a head indraft sonde. The ambient sonde is launched 2,3 km to the SE at 16:42 UTC. Profiles use a thin line for the ambient sonde and a thick line for the updraft representing Θv (K, red), Relative humidity (% blue), wind direction (°, violet), wind speed (m·s^{-1}, dark red) and vertical speed w (m·s-1, orange). The Θv profiles include LCL (dashed green). The parcel method for potential plume height by ML parcel (dashed pink vertical arrow) and MU parcel (dark dashed vertical arrow) is shown on the Θv. The RH (%) maximum value identifies the mixing layer height. The wind direction and speed profiles identify the wind shear. The rising velocity quantifies plume top heights (dashed orange line) Using the 2m·s^{-1} criteria. The horizontal thin and dashed grey line indicates the 300 m AGL needed to confirm an in-plume sonde as in Figure 7. Bottom table: wildfire information: Region, total and current hour burnt area (ha), launching hour for in-plume and ambient sonde, Fireline intensity (FLI, kW·m^{-1}), rate of spread (ROS, m·s^{-1}), heat flux captured by satellite infrared sensors (FRE, TJ), and the observed pyroconvection prototype as in Table 3.

https://doi.org/10.5194/egusphere-2025-1923
Preprint. Discussion started: 5 June 2025

3.3.3 Multiple launching during ongoing operations in active wildfires.

A set of updrafts and ambient pairs of sondes were launched at the Casablanca III fire in Chile (Figures 11 and 12). The fire grew up to 12073 ha between the 8th and 10th of February 2023. The situation in Chile was dramatic after the fires blew-up on February 2, resulting in over 362.000 ha burned.

Figure 11 shows two sondes launched one after the other from the same location (21:46 and 21:51 UTC) to try to assess plume height and deepening on top of the thick smoke layer from the burning since February 3rd (picture in Figure 11a). The plume top could only be seen far upwind from the fire (picture in Figure 11b), but not when inside the fire area.

The first sonde at 21:46 UTC shows an updraft excess of 14K on the Θv profile. The plume top is identified by the rising velocity profile at 2105 m AGL, confirmed by the RH proposed mixing layer (thick blue dashed line). The plume deepens 300 m on top of the ambient mixing layer (thin blue dashed line). The wind speed increases by 5 m·s^{-1} in the plume between 300 and 1200 m AGL. The rising velocity has an average of 10 m·s-1 above 300 m until the same 1200 m AGL that wind speed is modified. From there to the top, it gradually loses strength. This section of the vertical profile coincides with the height where the plume updraft temperature is already diluted, and the plume rises above its neutral buoyancy level.

The second sonde, launched five minutes later, recorded an updraft excess of 12K which dissipates more quickly and at a lower altitude compared to the first sonde. The plume top is identified by examining the vertical velocity and RH profiles at 1880 m AGL. This time, the rising velocity is weaker, averaging 6.3 m·s-1, and losing strength above the level of neutral buoyancy.

In both sondes, the MU parcel shows an unrealistic height potential if we do not account for the fast updraft temperature dilution. The ML parcel consistently provides a good assessment of the real plume height.

The plume height shows a difference of 225 m between the two measured plume top heights, signaling a plume just at ABL top or slightly overshooting on top of it, a resolution according to the variance of a turbulent plume top spatial and temporal resolution, as observed by radar and satellite measures (Lareau et al., 2024; Wilmot et al., 2022).

https://doi.org/10.5194/egusphere-2025-1923
Preprint. Discussion started: 5 June 2025

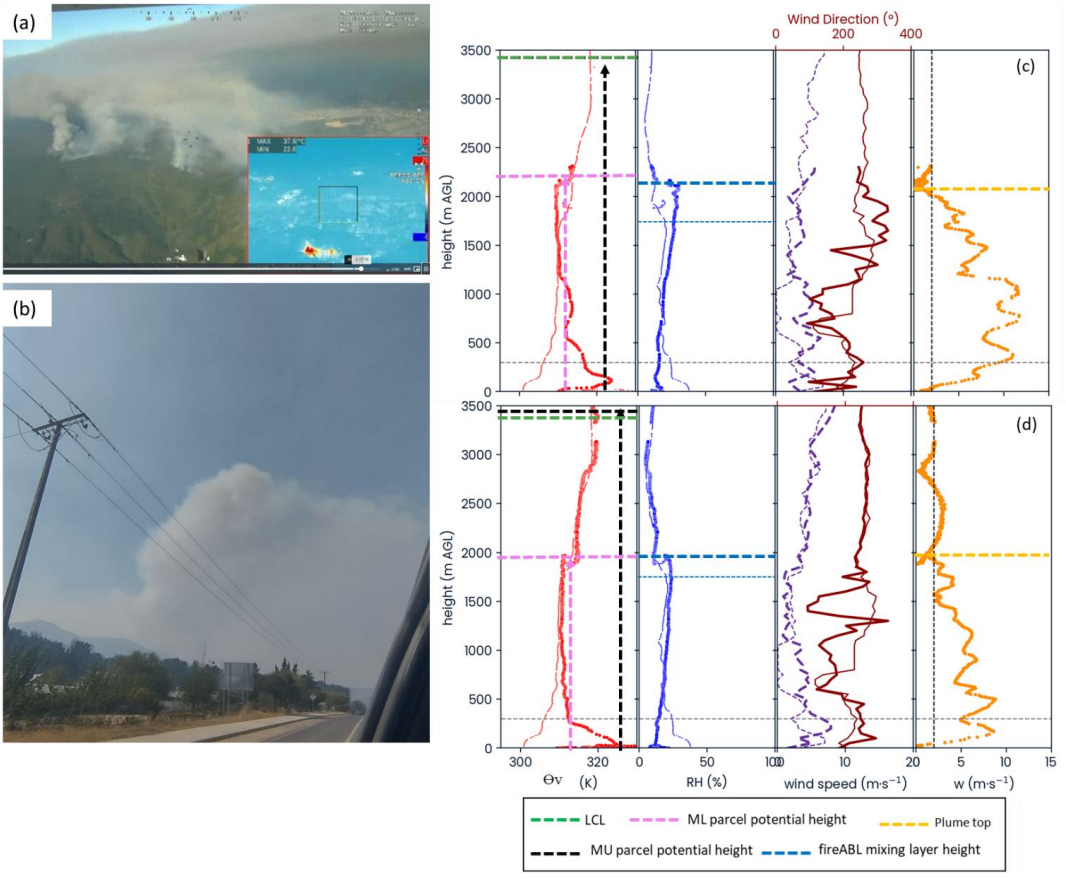

Fire event	Reg	Fuel	in-plume hour (UTC)	Ambient hour (UTC)	area (ha), (Total / hour)	FLI (kW·m⁻¹)	ROS (m·s⁻¹)	FRE (TJ)	Prototype
Casablanca III 08-02-2023	SA	TU/SH	21:46 21:51	22:27	12073 / 1012	19720	0.85	11.5	Convective

Figure 11: Interrelating state variable profiling for two consecutive sondes from the same launching site. The fire has a thick smoke layer covering Chile's central Valley after the fires from the 3rd of February (a) that already had consumed 425.000 ha. The plume of Casablanca fire can only be seen on the fringes of the thick smoke layer (b). c) Casablanca III fire the 8th of February at 21:46 UTC by a flank indraft sonde. d): Casablanca III fire the 8th of February at 21:51 UTC by a flank indraft sonde. The ambient sonde is launched 4,8 km to the E at 22:27 UTC. Profiles use a thin line for the ambient sonde and a thick line for the updraft representing Θv (K, red), Relative humidity (% blue), wind direction (°, violet), wind speed ($m \cdot s^{-1}$, dark red) and vertical speed w (m·s-1, orange). The Θv profiles include LCL (dashed green). The parcel method for potential plume height by ML parcel (dashed pink vertical arrow) and MU parcel (dark dashed vertical arrow) is shown on the Θv. The RH (%) maximum value identifies the mixing layer height. The wind direction and speed profiles identify the wind shear. The rising velocity quantifies plume top heights (dashed orange line) using the $2 m \cdot s^{-1}$ criteria. The horizontal thin and dashed grey line indicates the 300 m AGL needed to confirm an in-plume sonde as in Figure 7. Bottom table: wildfire information: Region, total and current hour burnt area (ha), launching hour for in-plume and ambient sonde, Fireline intensity (FLI, $kW \cdot m^{-1}$), rate of spread (ROS, $m \cdot s^{-1}$), heat flux captured by satellite infrared sensors (FRE, TJ), and the observed pyroconvection prototype as in Table 3.

The fire was already 8173 ha in size, and on the 10th of February 2023 increased in size by 3900 ha. It was assessed as a convective plume prototype without pyroCu transition being possible due to an ambient LCL 2000 m higher than ABL (Figure 12). Fire behavior was initially expected to calm in the early evening, but there was a 60% chance of intensification during the day-to-night transition due to the advection of drier air from the SW. The important takeout of the ambient-updraft sondes readings from the fireline are:

https://doi.org/10.5194/egusphere-2025-1923
Preprint. Discussion started: 5 June 2025

- At 20:03 UTC, the fire moves slowly after intense midday runs, with a shallow, diluted plume. A head indraft sonde profile shows a Θv spike of 12 K, producing a potential MU parcel rise to the LCL (green line). A more realistic parcel rise is identified by ML parcel at 930 m AGL. The rising velocity profile, however, measures a plume top just at 750 m AGL, according to the poor plume strength observed. The RH profile confirms no ABL height modification by the plume, a measurement that confirms the height of wind speed profile modification as well. Despite the current conditions, the situation is only sufficient to produce a weak surface plume prototype. However, it is unstable because the MU parcel has the potential to reach the LCL and force a transition to a moist pyroconvection prototype given enough fire spread to create intense updraft conditions in the plume.
- At 20:29 UTC, a new flank updraft sounding confirms that the reduction in burning intensity has stabilized, showing a much less intense potential temperature spike of 5 K. The ML parcel now shows a 1080 m AGL height, and MU reaches the potential height of 2600 m. The plume top of a weaker surface plume is measured at 600 m by the rising velocity, as confirmed by unmodified HR and wind speed profile between ambient and updraft conditions. The situation appears to be stabilizing; however, we must remain aware, as an increase in fire intensity could lead to the formation of a deeper plume, as suggested by the MU parcel.
- At 22:06 UTC, a reignition on the flank further south started a new intense run. A flank updraft sonde was launched, showing a Θv excess profile up to 1670 m AGL, and a rising velocity profile proposeing plume top at 1910 m AGL. The new fire now has a plume deepening more than three times the previous plume top. The measured plume height stays just below the ML parcel, deepening 500 m on top of the ambient ABL. This extreme is confirmed by the change in the RH profile and a modified wind speed profile up to the proposed plume top. The opening of the left flank is building an intense head fire using drier conditions advected into the area: the ambient RH decreased rapidly from 20% at 20:03 UTC to 8% at 22:06 UTC. Such a scenario proposes a convective plume height just 900 m below LCL. If the fire spread keeps its pace, we can assess a potential transition to an overshooting pyroCu prototype, as proposed by the unconstrained MU parcel potential height.

https://doi.org/10.5194/egusphere-2025-1923
Preprint. Discussion started: 5 June 2025

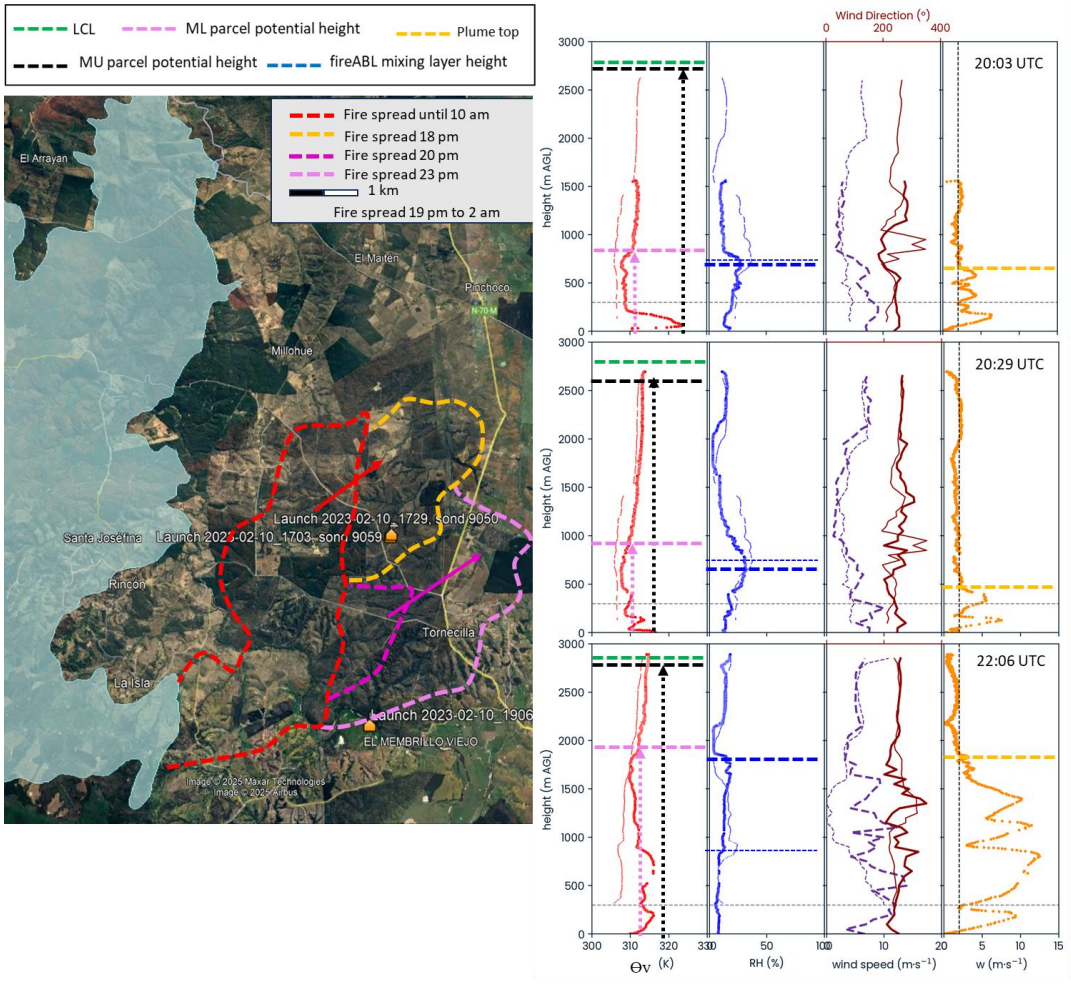

Fire event	Reg	Fuel	in-plume hour (UTC)	Ambient hour (UTC)	area (ha), (Total / hour)	FLI (kW·m^{-1})	ROS (m·s^{-1})	FRE (TJ)	Prototype
Casablanca III 10-02-2023	SA	TU/SH	20:03	20:56	12073 / 11.6	2800	0.08	1.02	Surface
Casablanca III 10-02-2023	SA	TU/SH	20:29	20:56	12073 / 6.2	1756	0.02	1.1	Surface
Casablanca III 10-02-2023	SA	TU/SH	22:06	22:30	12073/ 630	31114	1.1	7	Convective

Figure 12: Vertical profiling methodology applied during Casablanca III (Chile) fire, 10th February 2023. We show three updraft sondes (20:03 UTC, a head indraft, 20:29 UTC, and 22:06 UTC, a flank indraft) paired with two ambient sondes launched 7 km to the E at 20:56 and 22:30 UTC. Profiles use a thin line for the ambient sonde and a thick line for the updraft representing Θv (K, red), Relative humidity (% blue), wind direction (°, violet), wind speed (m·s-1, dark red) and vertical speed w (m·s-1, orange). The Θv profiles include LCL (dashed green). The parcel method for potential plume height by ML parcel (dashed pink vertical arrow) and MU parcel (dark dashed vertical arrow) is shown on the Θv. The RH (%) maximum value identifies the mixing layer height. The wind direction and speed profiles identify the wind shear. The rising velocity quantifies plume top heights (dashed orange line) Using the 2m·s^{-1} criteria. The horizontal thin and dashed grey line indicates the 300 m AGL needed to confirm an in-plume sonde as in Figure 7. Bottom table: wildfire information: Region, tatal and current hour burnt area (ha), launching hour for in-plume and ambient sonde, Fireline intensity (FLI, kW·m^{-1}), rate of spread (ROS, m·s^{-1}), heat flux captured by satellite infrared sensors (FRE, TJ), and the observed pyroconvection prototype as in Table 3.

3.4 Failed profiles

https://doi.org/10.5194/egusphere-2025-1923
Preprint. Discussion started: 5 June 2025

It is important to note that during the campaigns, we did not observe detrained sondes from the plume once the sonde entered the plume neck. However, we have had cases of sondes failing to enter the plume or entering the plume at higher altitudes when we launch into weak or intermittent indraft conditions. Those cases have always been reported with launching conditions too far away from the head fire (Figure S4) or when we launch into a decaying head fire, and there are strong surface winds present (>6 m·s-1).

4 Discussion

The methodology described enables the systematic collection of ambient and in-plume profile measurements and focuses on measuring changes in state variables induced by plumes relative to ambient conditions. This, in turn, enhances the understanding and modeling of pyroconvection. Firefighters can also use it to assess potential pyroconvection transitions in situ and in real-time. Below, we further elaborate on aspects related to the location of the sondes and the interpretation of the underlying physics.

4.1 Small balloon's reliability for capturing local profile characteristics.

In-situ ambient and updraft profiles measured with operational small balloons effectively reduced uncertainty from atmospheric model resolution by capturing local singularities that those models cannot account for (Dutra et al., 2021; Salvador et al., 2016; Wagner et al., 2014). Throughout our different campaigns, profiles with humidity advection were more prone to those local singularities than dry convection and stable profiles (Figure 3).

The novelty in our methodology comes from the systematic pairing of ambient and updraft profiles. They provide real-time measures for understanding how fire-atmosphere interaction is altering the ambient ABL thermodynamics. These profiles directly measure the plume current Θ and q values for the parcel potential rise, reducing the need to apply theoretical adjustments (Luderer et al., 2009; Potter, 2005). They also complement state-of-the-art methods (Artés et al., 2022; Leach and Gibson, 2021; Tory and Kepert, 2021).

However, it is important to note that with such small balloons, ambient sondes may not capture the full extent of the vertical profile in the presence of deep stability, subsidence, or wind speed shear. In these situations, the sondes tend to stabilize their ascent at the plume injection height layer. While it provides the necessary information, atmospheric models are sometimes needed to supplement data from above those layers (Eghdami et al., 2023).

4.2 Evaluating sonde data for capturing updraft variables and plume top

The comparison of state variables between updraft and ambient conditions helps in identifying plume-induced changes in the ambient conditions, assessing the plume height, and facilitating awareness of current pyroconvection conditions.

The Θv, despite its use for estimating updraft potential maximum height by the parcel method, is not sensitive enough to identify the plume top. The temperature increase in the updraft is quickly diluted before reaching 50% of the plume profile, coinciding with previous measurements (Charland and Clements, 2013; Kiefer et al., 2009). Above this height, non-buoyant deepening is driven by plume mass flux momentum (Moisseeva, 2020). The close to zero or even negative values from the updraft-ambient comparison cause this variable to poorly identify the plume top without the other variable's profile assessment. The dry convection case at Santa Ana (Figure 9b) exemplifies this situation. The Θv profile from the updraft deepening above the ambient ABL profile is 5 K cooler than ambient, failing to assess the plume top correctly by 580 m.

The updraft rising velocity profile allows us to better determine the plume top by identifying where dilution occurs. These profiles differ significantly from ambient rising velocity profiles. Additionally, radar data confirms that the sondes travel with the updraft, rather than strictly within the internal cores, as they ascend towards the top of the plume (Figure 8).

https://doi.org/10.5194/egusphere-2025-1923
Preprint. Discussion started: 5 June 2025

The measured rising velocity values of the updraft sondes, which reach up to 18 m·s⁻¹, are lower than the extreme updrafts of deep pyroconvective clouds (pyroCb) observed by Doppler radar, where peak velocities range between 30 and 60 m·s⁻¹ (Lareau et al., 2024; Rodriguez et al., 2020). It is important to note that these measurements are localized to a small section of a significantly large pyroCb plume that extends to a height above 10-12 km, but with average updrafts ranging from 8 to 18 m·s⁻¹. Other radar measurements reported rising velocity peaks between 7 and 21 m·s⁻¹ (Banta et al., 1992), aligning with modeling studies indicating maximum values of about 17 to 21 m·s⁻¹ (Zhang et al., 2019).

In our measurements, differences may stem from our strategy of focusing on fires during their initial stages. We focus on capturing the plume top and assessing firefighters with the pyroconvective prototype potential rather than focusing on maximum updraft core values in mature plumes. In such an approach, we capture plumes in their initial stages, around 1500 to 3000 m in height, mainly with a plume top located at the ABL top and deepening into the free troposphere. Those plumes lack the extreme cores as are measured with mature plumes (Lareau et al., 2024). Indeed, sondes traveling with the indraft flow into the updraft of a plume, may not enter the central plume cores and might instead travel in less intense updrafts that are present in the plume around the central cores, as illustrated by continuous radar measures (Lareau et al., 2024) and theorized by pyroconvective models (Freitas et al., 2009; Tory and Kepert, 2021). In the cases where our sondes were launched into developing pyroCu and pyroCb, they recorded rising velocity peaks of 18 and 21 m·s-1 when entering the pyrocloud (Figure S6).

4.3 Sensitivity of updraft profiles to the launching site with respect to the indraft origin

A key finding from our research is that the location where the in-plume sondes are launched—whether at the head, flank, or rear of the fire front—affects the profile of the state variables following the intensity and temperature differences between indraft origin flow with respect to the head fire detected in observations and simulations alike (Canfield et al., 2014; Clark et al., 1996). We observe distinct temperature spikes in the lower 50% of the head and flank indraft profile (see Figure 5c & d). In this case is important to notice the Θv excess temperature difference between head-indraft and rear-indraft profiles. It illustrates how the head fire creates updraft moving air that is rapidly replaced by the indraft mainly coming from behind the heat fires. This case highlights the value of in-plume sondes in providing research data to improve our pyroconvection plume dynamics.

The profile observed at the rear indraft (Figure 5b) reveals an apparent contradiction: despite displaying the best and fastest rising profile (Figure 6b), it has smaller differences in temperature (Θv) between the ambient and updraft values. This observation suggests that the rear indraft sonde measures a flow of fresh ambient air that enters the updraft without any temperature excess during the first half of the profile height. The observation is supported by previous works signaling the rear indraft as the most important and being formed by descending air into the plume neck base (Charland and Clements, 2013; Clark et al., 1996; Clements, 2010; Werth et al., 2011). This finding highlights the importance of our approach in delivering valuable research data.

These temperature spikes (head and flank indraft) and lack of temperature excess (rear indraft) pose challenges for calculating parcel methods and may lead to unrealistic parcel trajectories. Therefore, caution is required when applying the parcel method in the head fire and flank fire indrafts. Our observations indicate that the ML parcel method is the most suitable for raw sonde profile data (Leach and Gibson, 2021; Tory and Kepert, 2021). However, for fireline assessment, head and flank spikes may be considered the 'head-indraft' spikes to analyze worst-case scenarios (Figure 12).

4.4 Assessing pyroconvection prototypes transitions

The systematic pairing of ambient and updraft state variables improves the data for the understanding of fire-atmosphere coupling effects and the application of plume and pyroconvection models. The in-situ gathered data, by better characterizing the local ambient conditions, assessing the updraft buoyancy dilution and the current plume height using the updraft rising

https://doi.org/10.5194/egusphere-2025-1923
Preprint. Discussion started: 5 June 2025

velocity profile (Figure 5 and Figure 7), enhances the traditional fire manager's use of skew-T diagrams and parcel methods over the Θv profile (Goens and Andrews, Patricia L, 1998; Leach and Gibson, 2021; Tory and Kepert, 2021). We can acquire an awareness of the difference between the current measured plume height, the potential height in the current profile by the parcel method and the height needed for transitioning to a deeper pyroconvection prototype. Additionally, profiles of relative humidity (RH), wind direction, and wind speed contribute to our analysis by illustrating to what extent the fire-atmosphere interactions are changing and deepening the ABL into a fire dominated fireABL and whether the wind is dominating and tilting the plume or it is the plume itself that is modifying the wind shear level height (Figure 12).

The real-time in-situ measurements enable a better management of both sources of uncertainty for firefighters (Castellnou et al., 2019): those related to fire-induced changes (Figure 9 and 10) and those related to advected changes in the ABL (Figure 4 and 12).

The plume top assessment using simultaneous sondes (Figure 11) validates the pyroconvection analysis, even when entrainment turbulence at the boundary layer top may interfere with the sondes reading. The methodology demonstrates that the plume top is dynamic. The variability in measurements is consistent with those obtained from other methods, such as radar and satellites. We should consider this variability to account for transitions in the pyroconvection prototype.

The different cases analyzed indicated that the pyroconvection transition is highly sensitive to the plume updraft strength (Figure 9 and 10). The updraft strength is closely tied to surface fire activity, defined by front size and depth, as supported by plume model analyses in the literature (Badlan et al., 2021; Rio et al., 2010). The bigger the front feeding the plume, the more protected from detrainment and the less diluted the plume core in its ascend, and because of that, the deeper the plume penetrates into the free troposphere (Liu et al., 2010, 2012).

Linking pyroconvection potential provided by our methodology to observed front size allows firefighters to directly assess how changes in front size will change pyroconvection prototype and ultimately affect fire spread. Such in-situ information adds a new capability to detect a common type of fire resulting in fatalities (Page et al., 2019): small fires that can suddenly transition and blow up without changes induced by new advected ambient conditions. They are not limited by atmospheric vertical profile thermodynamics but by the flaming front not providing the updraft strength to travel undiluted to the LCL height and trigger a pyroconvection prototype transition. In such fires, a change in slope, fuel, or another factor can induce the plume updraft strength to deepen and create the thermodynamic changes for a pyroconvection prototype transition, ultimately changing fire spread unexpectedly (see Martorell case in Figure 10) threatening firefighters on the fireline.

4.5 Limitations

Gathering data directly from within a fire environment poses challenges to the safety of the launching team and the reliability of the data collected. Our method has three potential limitations.

First, verifying whether the data obtained from the sonde is adequate for use as an in-plume or environmental profile is important. These sondes must ascend an average of 300 meters (as illustrated in Figure 6) to properly position them in the updraft. This limitation directly affects our ability to assess the plume's height if it does not rise above the minimum required level or the plume strength is too weak to separate its rising velocity values from ambient ones easily.

Secondly, well-established large fires can have multiple updraft (Liu et al., 2010) that can achieve different pyroconvection profiles. With our method, we can only assess the updraft over the plume that our sonde has ascended.

Lastly, it is crucial to account for temperature spikes in the sonde's initial ascent path, particularly in flank and head indraft profiles when using this data for modeling; otherwise, numerical computations of Rib and fireCAPE may be inaccurate.

Launching multiple sondes can address all three limitations (see Figure 11).

https://doi.org/10.5194/egusphere-2025-1923
Preprint. Discussion started: 5 June 2025

5 Conclusions

We present a new observational method and strategy aimed at improving our understanding of fire plume dynamics and their interactions with the surrounding environment. The method is based on simultaneous sounding observational profiles of in-plume wildfires and their surrounding ambient. These profile observations enable us to complete a description of the main dynamic characteristics of the fire plume with respect to the ABL characteristics and classify the fires according to pyroconvection prototype categories.

Despite the limitations of sondes as a single trajectory inside the plume, the results from 156 updraft-launched sondes offer robust evidence for reliably detecting plume top heights using the sonde rising velocity, wind, potential temperature, and humidity profiles.

Compared to previous radiosonde applications in areas affected by fires, the novelty of this approach lies in the systematic and simultaneous collection of data from ambient conditions and updraft profiles within the plume. By employing this dual-sounding method, we gather observations of the fire-atmosphere dynamic interactions in almost real time. This coupling is missing in atmospheric models. More specifically, our observations and analysis enable us to quantify the rapid vertical variations in moisture and wind profiles driven by land-sea contrasts, topography, frontal advection, and their interaction with the fire. This insitu quantification is crucial for assessing potential transitions to deeper convection, which may drive extreme fire behavior.

Our new methodology of in-plume radiosonde profiling of state variables provides a cost-effective and essential complement to current assessment methods. It enhances the understanding of fire-atmosphere dynamics in-situ and in-real time, thereby reducing uncertainty and increasing safety for firefighters confronting increasingly intense wildfire events worldwide.

Data availability

Final Dataset in EWED project data portal: http://wildfiredataportal.eu/

The profiles in the Figures are in DOI **10.5281/zenodo.15264835**

Funding

This project has received funding from Directorate-General for European Civil Protection and Humanitarian Aid Operations (ECHO) through the project EWED (101140363), and the Horizon 2020 research and innovation program under grant agreements No 101037419 (FIRE-RES).

Conflicts of interest

The authors declare that they have no conflict of interest.

Authors contribution

MC, MM, MB, BR planned the campaign; MC, MB, BR, JP, LE, BV, and PG conceptualized the methodology and performed the measurements; MC, MB, PG, and JV analyzed the data; MC wrote the manuscript draft; JV, MJ, CVH, TR, CS, MB, PG, BB, and JP reviewed and edited the manuscript.

https://doi.org/10.5194/egusphere-2025-1923
Preprint. Discussion started: 5 June 2025

Acknowledgments

The authors gratefully acknowledge the Servei Meteorològic de Catalunya (SMC, www.meteo.cat) for providing access to radar data used in this study.

We thank Antonio Ariza and Alex Sancho for adapting the radiosonde equipment to the fire service operational vehicles to launch the radiosondes at wildfires efficiently. We also thank Jorge Saavedra from CONAF for facilitating extra data collection in the Chile wildfire campaigns. Additionally, we thank Jose Cespedes for arranging the necessary helium and equipment. Finally, we thank Vicor Lopez for documenting the launching procedure with imagery.

References

Pyrocumulonimbus - Glossary of Meteorology: https://glossary.ametsoc.org/wiki/Pyrocumulonimbus, last access: 25 October 2023.

Artés, T., Castellnou, M., Houston Durrant, T., and San-Miguel, J.: Wildfire–atmosphere interaction index for extreme-fire behaviour, Natural Hazards and Earth System Sciences, 22, 509–522, https://doi.org/10.5194/nhess-22-509-2022, 2022.

Badlan, R. L., Sharples, J. J., Evans, J. P., McRae, R. H. D., Badlan, R. L., Sharples, J. J., Evans, J. P., and McRae, R. H. D.: Factors influencing the development of violent pyroconvection. Part I: fire size and stability, Int. J. Wildland Fire, 30, 484–497, https://doi.org/10.1071/WF20040, 2021.

Banta, R. M., Olivier, L. D., Holloway, E. T., Kropfli, R. A., Bartram, B. W., Cupp, R. E., and Post, M. J.: Smoke-Column Observations from Two Forest Fires Using Doppler Lidar and Doppler Radar, Journal of Applied Meteorology and Climatology, 31, 1328–1349, https://doi.org/10.1175/1520-0450(1992)031<1328:SCOFTF>2.0.CO;2, 1992.

Benik, J., Farguell, A., Mirocha, J., Clements, C., and Kochanski, A.: Analysis of Fire-Induced Circulations during the FireFlux2 Experiment, Fire, 6, 332, https://doi.org/10.3390/fire6090332, 2023.

Bessardon, G. E. Q., Fosu-Amankwah, K., Petersson, A., and Brooks, B. J.: Evaluation of Windsond S1H2 performance in Kumasi during the 2016 DACCIWA field campaign, Atmospheric Measurement Techniques, 12, 1311–1324, https://doi.org/10.5194/amt-12-1311-2019, 2019.

Bolton, D.: The Computation of Equivalent Potential Temperature, Monthly Weather Review, 108, 1046–1053, https://doi.org/10.1175/1520-0493(1980)108<1046:TCOEPT>2.0.CO;2, 1980.

Brewer, M. J. and Clements, C. B.: Meteorological Profiling in the Fire Environment Using UAS, Fire, 3, 36, https://doi.org/10.3390/fire3030036, 2020.

Butler, B. W.: Wildland firefighter safety zones: a review of past science and summary of future needs, Int. J. Wildland Fire, 23, 295–308, https://doi.org/10.1071/WF13021, 2014.

Canfield, J. M., Linn, R. R., Sauer, J. A., Finney, M., and Forthofer, J.: A numerical investigation of the interplay between fireline length, geometry, and rate of spread, Agricultural and Forest Meteorology, 189–190, 48–59, https://doi.org/10.1016/j.agrformet.2014.01.007, 2014.

Cardil, A. and Molina, D. M.: Factors Causing Victims of Wildland Fires in Spain (1980–2010), Human and Ecological Risk Assessment: An International Journal, 21, 67–80, https://doi.org/10.1080/10807039.2013.871995, 2015.

Castellnou, M., Prat-Guitart, N., Arilla, E., Larrañaga, A., Nebot, E., Castellarnau, X., Vendrell, J., Pallàs, J., Herrera, J., Monturiol, M., Cespedes, J., Pagès, J., Gallardo, C., and Miralles, M.: Empowering strategic decision-making for wildfire management: avoiding the fear trap and creating a resilient landscape, Fire Ecology, 15, https://doi.org/10.1186/s42408-019-0048-6, 2019.

Castellnou, M., Bachfischer, M., Miralles, M., Ruiz, B., Stoof, C. R., and Arellano, J. V.-G. de: Pyroconvection Classification based on Atmospheric Vertical Profiling Correlation with Extreme Fire Spread Observations, https://doi.org/10.1029/2022JD036920, 2022.

https://doi.org/10.5194/egusphere-2025-1923
Preprint. Discussion started: 5 June 2025

Charland, A. M. and Clements, C. B.: Kinematic structure of a wildland fire plume observed by Doppler lidar, Journal of Geophysical Research: Atmospheres, 118, 3200–3212, https://doi.org/10.1002/jgrd.50308, 2013.

Clark, T. L., Jenkins, M. A., Coen, J., and Packham, D.: A Coupled Atmosphere– Fire Model: Convective Feedback on Fire-Line Dynamics, Journal of Applied Meteorology and Climatology, 35, 875–901, https://doi.org/10.1175/1520-0450(1996)035<0875:ACAMCF>2.0.CO;2, 1996.

Clements, C. B.: Thermodynamic structure of a grass fire plume, Int. J. Wildland Fire, 19, 895–902, https://doi.org/10.1071/WF09009, 2010.

Clements, C. B., Lareau, N. P., Seto, D., Contezac, J., Davis, B., Teske, C., Zajkowski, T. J., Hudak, A. T., Bright, B. C., Dickinson, M. B., Butler, B. W., Jimenez, D., and Hiers, J. K.: Fire weather conditions and fire–atmosphere interactions observed during low-intensity prescribed fires – RxCADRE 2012, Int. J. Wildland Fire, 25, 90–101, https://doi.org/10.1071/WF14173, 2015.

Clements, C. B., Lareau, N. P., Kingsmill, D. E., Bowers, C. L., Camacho, C. P., Bagley, R., and Davis, B.: The Rapid Deployments to Wildfires Experiment (RaDFIRE): Observations from the Fire Zone, Bulletin of the American Meteorological Society, 99, 2539–2559, https://doi.org/10.1175/BAMS-D-17-0230.1, 2018.

Clements, C. B., Kochanski, A. K., Seto, D., Davis, B., Camacho, C., Lareau, N. P., Contezac, J., Restaino, J., Heilman, W. E., Krueger, S. K., Butler, B., Ottmar, R. D., Vihnanek, R., Flynn, J., Filippi, J.-B., Barboni, T., Hall, D. E., Mandel, J., Jenkins, M. A., O'Brien, J., Hornsby, B., and Teske, C.: The FireFlux II experiment: a model-guided field experiment to improve understanding of fire–atmosphere interactions and fire spread, Int. J. Wildland Fire, 28, 308–326, https://doi.org/10.1071/WF18089, 2019.

Couto, F. T., Filippi, J.-B., Baggio, R., Campos, C., and Salgado, R.: Triggering Pyro-Convection in a High-Resolution Coupled Fire–Atmosphere Simulation, Fire, 7, 92, https://doi.org/10.3390/fire7030092, 2024.

Cruz, M. G., Sullivan, A. L., Gould, J. S., Sims, N. C., Bannister, A. J., Hollis, J. J., and Hurley, R. J.: Anatomy of a catastrophic wildfire: The Black Saturday Kilmore East fire in Victoria, Australia, Forest Ecology and Management, 284, 269–285, https://doi.org/10.1016/j.foreco.2012.02.035, 2012.

Cunningham, C. X., Williamson, G. J., and Bowman, D. M. J. S.: Increasing frequency and intensity of the most extreme wildfires on Earth, Nat Ecol Evol, 1–6, https://doi.org/10.1038/s41559-024-02452-2, 2024.

Di Virgilio, G., Evans, J. P., Blake, S. A. P., Armstrong, M., Dowdy, A. J., Sharples, J., and McRae, R.: Climate Change Increases the Potential for Extreme Wildfires, Geophysical Research Letters, 46, 8517–8526, https://doi.org/10.1029/2019GL083699, 2019.

Duane, A., Castellnou, M., Bachfisher, M., and Brotons, L.: Fire Rate of Spread and Growth Rate in a Set of 30 Global Wildfires: New Evidence of Extreme Fire Behavior, JOURNAL OF ENVIRONMENTAL INFORMATICS, 44, 87–99, 2024.

Dutra, E., Johannsen, F., and Magnusson, L.: Late Spring and Summer Subseasonal forecasts in the Northern Hemisphere midlatitudes: biases and skill in the ECMWF model, Monthly Weather Review, https://doi.org/10.1175/MWR-D-20-0342.1, 2021.

Eghdami, M., Juliano, T. W., Jiménez, P. A., Kosovic, B., Castellnou, M., Kumar, R., and Vila-Guerau de Arellano, J.: Characterizing the Role of Moisture and Smoke on the 2021 Santa Coloma de Queralt Pyroconvective Event Using WRF-Fire, Journal of Advances in Modeling Earth Systems, 15, e2022MS003288, https://doi.org/10.1029/2022MS003288, 2023.

Finney, M. A., Cohen, J. D., Forthofer, J. M., McAllister, S. S., Gollner, M. J., Gorham, D. J., Saito, K., Akafuah, N. K., Adam, B. A., and English, J. D.: Role of buoyant flame dynamics in wildfire spread, Proceedings of the National Academy of Sciences, 112, 9833–9838, https://doi.org/10.1073/pnas.1504498112, 2015.

Finney, M. A., McAllister, S. S., Forthofer, J. M., and Grumstrup, T. P.: Wildland Fire Behaviour: Dynamics, Principles and Processes, Csiro Publishing, 377 pp., 2021.

Freitas, S. R., Longo, K. M., Chatfield, R., Latham, D., Silva Dias, M. a. F., Andreae, M. O., Prins, E., Santos, J. C., Gielow, R., and Carvalho, J. A. J.: Including the sub-grid scale plume rise of vegetation fires in low resolution atmospheric transport models, Atmospheric Chemistry and Physics, 7, 3385–3398, https://doi.org/10.5194/acp-7-3385-2007, 2007.

Freitas, S. R., Longo, K., Trentmann, J., and Latham, D.: Including the environmental wind effects on smoke plume rise of vegetation fires in 1D cloud models, in: Proceedings of the Eighth Symposium on Fire and Forest Meteorology, 2009.

https://doi.org/10.5194/egusphere-2025-1923
Preprint. Discussion started: 5 June 2025

Fromm, M., Servranckx, R., Stocks, B. J., and Peterson, D. A.: Understanding the critical elements of the pyrocumulonimbus storm sparked by high-intensity wildland fire, Commun Earth Environ, 3, 1–7, https://doi.org/10.1038/s43247-022-00566-8, 2022.

Gleason, P.: LCES -- a key to safety in the wildland fire environment, Fire Management Notes, 52, 1991.

Goens, D. W. and Andrews, Patricia L: Weather and fire behavior factors related to the 1990 Dude Fire near Payson, Arizona, in: Proceedings: 2nd symposium on fire and forest meteorology, American Meteorological Society, Boston, MA, 153–158, 1998.

Haines, D. A.: A lower atmosphere severity index for wildlife fires, National Weather Digest, 13, 23–27, 1989.

Heilman, W. E.: Atmospheric turbulence and wildland fires: a review, Int. J. Wildland Fire, 32, 476–495, https://doi.org/10.1071/WF22053, 2023.

Holzworth, G. C.: Estimates of mean maximum mixing depths in the contiguous United States, Monthly Weather Review, 92, 235–242, https://doi.org/10.1175/1520-0493(1964)092<0235:EOMMMD>2.3.CO;2, 1964.

Jenkins, M.: Investigating the Haines Index using parcel model theory, International Journal of Wildland Fire, 13, 297–309, https://doi.org/10.1071/WF03055, 2004.

Kiefer, M. T., Parker, M. D., and Charney, J. J.: Regimes of Dry Convection above Wildfires: Idealized Numerical Simulations and Dimensional Analysis, Journal of the Atmospheric Sciences, 66, 806–836, https://doi.org/10.1175/2008JAS2896.1, 2009.

Koch, S. E., Fengler, M., Chilson, P. B., Elmore, K. L., Argrow, B., Andra, D. L., and Lindley, T.: On the Use of Unmanned Aircraft for Sampling Mesoscale Phenomena in the Preconvective Boundary Layer, Journal of Atmospheric and Oceanic Technology, 35, 2265–2288, https://doi.org/10.1175/JTECH-D-18-0101.1, 2018.

Kochanski, A. K., Mallia, D. V., Fearon, M. G., Mandel, J., Souri, A. H., and Brown, T.: Modeling Wildfire Smoke Feedback Mechanisms Using a Coupled Fire-Atmosphere Model With a Radiatively Active Aerosol Scheme, Journal of Geophysical Research: Atmospheres, 124, 9099–9116, https://doi.org/10.1029/2019JD030558, 2019.

Lahaye, S., Curt, T., Fréjaville, T., Sharples, J., Paradis, L., and Hély, C.: What are the drivers of dangerous fires in Mediterranean France?, Int. J. Wildland Fire, 27, 155–163, https://doi.org/10.1071/WF17087, 2018.

Lareau, N. P. and Clements, C. B.: Environmental controls on pyrocumulus and pyrocumulonimbus initiation and development, Atmospheric Chemistry and Physics, 16, 4005–4022, https://doi.org/10.5194/acp-16-4005-2016, 2016.

Lareau, N. P., Donohoe, A., Roberts, M., and Ebrahimian, H.: Tracking Wildfires With Weather Radars, Journal of Geophysical Research: Atmospheres, 127, e2021JD036158, https://doi.org/10.1029/2021JD036158, 2022.

Lareau, N. P., Clements, C. B., Kochanski, A., Aydell, T., Hudak, A. T., McCarley, T. R., and Ottmar, R.: Observations of a rotating pyroconvective plume, Int. J. Wildland Fire, 33, https://doi.org/10.1071/WF23045, 2024.

Leach, R. N. and Gibson, C. V.: Assessing the Potential for Pyroconvection and Wildfire Blow Ups, J. Operational Meteor., 47–61, https://doi.org/10.15191/nwajom.2021.0904, 2021.

Li, H., Liu, B., Ma, X., Jin, S., Ma, Y., Zhao, Y., and Gong, W.: Evaluation of retrieval methods for planetary boundary layer height based on radiosonde data, Atmospheric Measurement Techniques, 14, 5977–5986, https://doi.org/10.5194/amt-14-5977-2021, 2021.

Liu, Y., Achtemeier, G. L., Goodrick, S. L., and Jackson, W. A.: Important parameters for smoke plume rise simulation with Daysmoke, Atmospheric Pollution Research, 1, 250–259, https://doi.org/10.5094/APR.2010.032, 2010.

Liu, Y., Goodrick, S. L., Achtemeier, G. L., Forbus, K., and Combs, D.: Smoke plume height measurement of prescribed burns in the south-eastern United States, Int. J. Wildland Fire, 22, 130–147, https://doi.org/10.1071/WF11072, 2012.

Luderer, G., Trentmann, J., Andreae, M. O., Luderer, G., Trentmann, J., and Andreae, M. O.: A new look at the role of fire-released moisture on the dynamics of atmospheric pyro-convection, Int. J. Wildland Fire, 18, 554–562, https://doi.org/10.1071/WF07035, 2009.

May, R. M., Goebbert, K. H., Thielen, J. E., Leeman, J. R., Camron, M. D., Bruick, Z., Bruning, E. C., Manser, R. P., Arms, S. C., and Marsh, P. T.: MetPy: A Meteorological Python Library for Data Analysis and Visualization, Bulletin of the American Meteorological Society, 103, E2273–E2284, https://doi.org/10.1175/BAMS-D-21-0125.1, 2022.

https://doi.org/10.5194/egusphere-2025-1923
Preprint. Discussion started: 5 June 2025

McCarthy, N., Guyot, A., Dowdy, A., and McGowan, H.: Wildfire and Weather Radar: A Review, Journal of Geophysical Research: Atmospheres, 124, 266–286, https://doi.org/10.1029/2018JD029285, 2019.

McCutchan, M. H.: Second AMS Conference on Mountain Meteorology 9-12 November 1981, Steamboat Springs, Colo., Bulletin of the American Meteorological Society, 63, 767–772, 1982.

McRae, R. H. D., Sharples, J. J., and Fromm, M.: Linking local wildfire dynamics to pyroCb development, Natural Hazards and Earth System Sciences, 15, 417–428, https://doi.org/10.5194/nhess-15-417-2015, 2015.

Moisseeva, N.: A numerical perspective on wildfire plume-rise dynamics, University of British Columbia, https://doi.org/10.14288/1.0395299, 2020.

Page, W. G., Freeborn, P. H., Butler, B. W., and Jolly, W. M.: A review of US wildland firefighter entrapments: trends, important environmental factors and research needs, Int. J. Wildland Fire, 28, 551, https://doi.org/10.1071/WF19022, 2019.

Paugam, R., Wooster, M., Freitas, S., and Val Martin, M.: A review of approaches to estimate wildfire plume injection height within large-scale atmospheric chemical transport models, Atmospheric Chemistry and Physics, 16, 907–925, https://doi.org/10.5194/acp-16-907-2016, 2016.

Peterson, D. A., Hyer, E. J., Campbell, J. R., Solbrig, J. E., and Fromm, M. D.: A Conceptual Model for Development of Intense Pyrocumulonimbus in Western North America, Monthly Weather Review, 145, 2235–2255, https://doi.org/10.1175/MWR-D-16-0232.1, 2017.

Potter: The Haines Index – it's time to revise it or replace it, Int. J. Wildland Fire, 27, 437–440, https://doi.org/10.1071/WF18015, 2018.

Potter, B. E.: The role of released moisture in the atmospheric dynamics associated with wildland fires, Int. J. Wildland Fire, 14, 77–84, https://doi.org/10.1071/WF04045, 2005.

Potter, B. E. and Anaya, M. A.: A Wildfire-relevant climatology of the convective environment of the United States, Int. J. Wildland Fire, 24, 267–275, https://doi.org/10.1071/WF13211, 2015.

Prichard, S., Larkin, N. S., Ottmar, R., French, N. H. F., Baker, K., Brown, T., Clements, C., Dickinson, M., Hudak, A., Kochanski, A., Linn, R., Liu, Y., Potter, B., Mell, W., Tanzer, D., Urbanski, S., and Watts, A.: The Fire and Smoke Model Evaluation Experiment—A Plan for Integrated, Large Fire–Atmosphere Field Campaigns, Atmosphere, 10, 66, https://doi.org/10.3390/atmos10020066, 2019.

Rio, C., Hourdin, F., and Chédin, A.: Numerical simulation of tropospheric injection of biomass burning products by pyro-thermal plumes, Atmospheric Chemistry and Physics, 10, 3463–3478, https://doi.org/10.5194/acp-10-3463-2010, 2010.

Rodriguez, B., Lareau, N. P., Kingsmill, D. E., and Clements, C. B.: Extreme Pyroconvective Updrafts During a Megafire, Geophysical Research Letters, 47, e2020GL089001, https://doi.org/10.1029/2020GL089001, 2020.

Romps, D. M.: Exact Expression for the Lifting Condensation Level, Journal of the Atmospheric Sciences, 74, 3891–3900, https://doi.org/10.1175/JAS-D-17-0102.1, 2017.

Rothermel, R. C.: Predicting behavior and size of crown fires in the northern Rocky Mountains, Res. Pap. INT-438. Ogden, UT: U.S. Department of Agriculture, Forest Service, Intermountain Research Station. 46 p., 438, https://doi.org/10.2737/INT-RP-438, 1991.

Salvador, N., Reis, N. C., Santos, J. M., Albuquerque, T. T. de A., Loriato, A. G., Delbarre, H., Augustin, P., Sokolov, A., and Moreira, D. M.: Evaluation of weather research and forecasting model parameterizations under sea-breeze conditions in a North Sea coastal environment, J Meteorol Res, 30, 998–1018, https://doi.org/10.1007/s13351-016-6019-9, 2016.

Scott, J. H. and Burgan, R. E.: Standard Fire Behavior Fuel Models: A Comprehensive Set for Use with Rothermel's Surface Fire Spread Model, U.S. Department of Agriculture, Forest Service, Rocky Mountain Research Station, 84 pp., 2005.

Seibert, P., Beyrich, F., Gryning, S.-E., Joffre, S., Rasmussen, A., and Tercier, P.: Review and intercomparison of operational methods for the determination of the mixing height, Atmospheric Environment, 34, 1001–1027, https://doi.org/10.1016/S1352-2310(99)00349-0, 2000.

Stratum, B. J. H. van, Arellano, J. V.-G. de, Heerwaarden, C. C. van, and Ouwersloot, H. G.: Subcloud-Layer Feedbacks Driven by the Mass Flux of Shallow Cumulus Convection over Land, Journal of the Atmospheric Sciences, 71, 881–895, https://doi.org/10.1175/JAS-D-13-0192.1, 2014.

https://doi.org/10.5194/egusphere-2025-1923
Preprint. Discussion started: 5 June 2025

Tory, K. J. and Kepert, J. D.: Pyrocumulonimbus Firepower Threshold: Assessing the Atmospheric Potential for pyroCb, Weather and Forecasting, 36, 439–456, https://doi.org/10.1175/WAF-D-20-0027.1, 2021.

Tory, K. J., Thurston, W., and Kepert, J. D.: Thermodynamics of Pyrocumulus: A Conceptual Study, Monthly Weather Review, 146, 2579–2598, https://doi.org/10.1175/MWR-D-17-0377.1, 2018.

Turco, M., Rosa-Cánovas, J. J., Bedia, J., Jerez, S., Montávez, J. P., Llasat, M. C., and Provenzale, A.: Exacerbated fires in Mediterranean Europe due to anthropogenic warming projected with non-stationary climate-fire models, Nat Commun, 9, 3821, https://doi.org/10.1038/s41467-018-06358-z, 2018.

Vilà-Guerau de Arellano, J., van Heerwaarden, C. C., van Stratum, B. J. H., and van den Dries, K.: Atmospheric Boundary Layer: Integrating Air Chemistry and Land Interactions, Cambridge University Press, Cambridge, https://doi.org/10.1017/CBO9781316117422, 2015.

Wagner, J. S., Gohm, A., and Rotach, M. W.: The Impact of Horizontal Model Grid Resolution on the Boundary Layer Structure over an Idealized Valley, Monthly Weather Review, 142, 3446–3465, https://doi.org/10.1175/MWR-D-14-00002.1, 2014.

Werth, P. A., Potter, B. E., Clements, C. B., Finney, M. A., Goodrick, S. L., Alexander, M. E., Cruz, M. G., Forthofer, J. A., and McAllister, S. S.: Synthesis of knowledge of extreme fire behavior: volume I for fire managers, U.S. Department of Agriculture, Forest Service, Pacific Northwest Research Station, Portland, OR, https://doi.org/10.2737/PNW-GTR-854, 2011.

Wilmot, T. Y., Mallia, D. V., Hallar, A. G., and Lin, J. C.: Wildfire plumes in the Western US are reaching greater heights and injecting more aerosols aloft as wildfire activity intensifies, Sci Rep, 12, 12400, https://doi.org/10.1038/s41598-022-16607-3, 2022.

Wilson, C. C.: Fatal and Near-fatal Forest Fires. The commom denominators, The International Fire Chief, 43, 12–15, 1977.

Wooster, M. J., Roberts, G. J., Giglio, L., Roy, D. P., Freeborn, P. H., Boschetti, L., Justice, C., Ichoku, C., Schroeder, W., Davies, D., Smith, A. M. S., Setzer, A., Csiszar, I., Strydom, T., Frost, P., Zhang, T., Xu, W., de Jong, M. C., Johnston, J. M., Ellison, L., Vadrevu, K., Sparks, A. M., Nguyen, H., McCarty, J., Tanpipat, V., Schmidt, C., and San-Miguel-Ayanz, J.: Satellite remote sensing of active fires: History and current status, applications and future requirements, Remote Sensing of Environment, 267, 112694, https://doi.org/10.1016/j.rse.2021.112694, 2021.

Zhang, Y., Gao, Z., Li, D., Li, Y., Zhang, N., Zhao, X., and Chen, J.: On the computation of planetary boundary-layer height using the bulk Richardson number method, Geoscientific Model Development, 7, 2599–2611, https://doi.org/10.5194/gmd-7-2599-2014, 2014.

Zhang, Y., Fan, J., Logan, T., Li, Z., and Homeyer, C. R.: Wildfire Impact on Environmental Thermodynamics and Severe Convective Storms, Geophysical Research Letters, 46, 10082–10093, https://doi.org/10.1029/2019GL084534, 2019.

Ziegler, J. A.: The Story Behind an Organizational List: A Genealogy of Wildland Firefighters' 10 Standard Fire Orders, Communication Monographs, 74, 415–442, https://doi.org/10.1080/03637750701716594, 2007.